

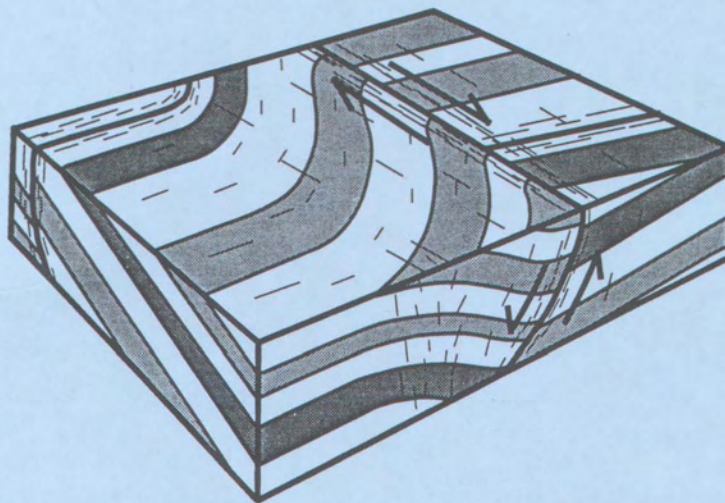
BEDROCK GEOLOGIC MAPS, AND FRACTURE AND
FAULT DATA FOR PORTIONS OF THE COKESBURY
AND NEW HILL 7.5-MINUTE QUADRANGLES,
DEEP RIVER TRIASSIC BASIN, WAKE COUNTY,
NORTH CAROLINA

by

Richard M. Wooten

Timothy W. Clark

Timothy L. Davis



NORTH CAROLINA GEOLOGICAL SURVEY
OPEN-FILE REPORT 96-3

DIVISION OF LAND RESOURCES
DEPARTMENT OF ENVIRONMENT, HEALTH
AND NATURAL RESOURCES

**BEDROCK GEOLOGIC MAPS, AND FRACTURE AND FAULT DATA
FOR PORTIONS OF THE COKESBURY AND NEW HILL
7.5-MINUTE QUADRANGLES,
DEEP RIVER TRIASSIC BASIN, WAKE COUNTY,
NORTH CAROLINA**

by

Richard M. Wooten

Timothy W. Clark

North Carolina Geological Survey
P.O. Box 27687
Raleigh, NC 27611-7687

Timothy L. Davis¹

North Carolina Geological Survey
P.O. Box 27687
Raleigh, NC 27611-7687

¹Now with: Exxon Production Research Company
P.O. Box 2189
Houston, TX 77252-2189

**NORTH CAROLINA GEOLOGICAL SURVEY
OPEN-FILE REPORT 96-3**

**DIVISION OF LAND RESOURCES
Charles H. Gardner
Director and State Geologist**

RALEIGH

1996

STATE OF NORTH CAROLINA
JAMES B. HUNT, JR., GOVERNOR

DEPARTMENT OF ENVIRONMENT,
HEALTH AND NATURAL RESOURCES
JONATHAN B. HOWES, SECRETARY

CONTENTS

	<u>Page</u>
Abstract	1
Introduction	1
Regional Overview	2
Previous and Ongoing Studies	6
Methods	6
General Stratigraphy	9
Structure	9
Bedding Orientation.....	9
Faults	10
South Borrow Pit Fault	10
Fault A	11
Fault B	16
Fault C	16
Fractures	18
General Fracture Characteristics	18
Fracture Trace Mapping	20
Hanging wall structures	23
Footwall Structures	24
Discussion	25
Stage 1	26
Stage 2	26
Stage 2 Normal Faulting	26
Stage 2 Strike-slip Faulting	28
Kinematic Model	29
Summary	30
Acknowledgements	31
References Cited	32
Appendix A: Structure data for the north and south borrow pits.....	36
Appendix B: Structure data for fracture trace map at location 4.....	43
Appendix C: Weathering and Rock Mass Classification	44

FIGURES

Figure 1. Physiographic provinces and Triassic rift basins of North Carolina and location of study area.....	3
Figure 2. Generalized geologic map (post-Triassic) of the southern Durham Triassic basin with study area and 7.5-minute quadrangles outlined.....	4
Figure 3. Data location map (1:6,000 scale) of the north and south borrow pits.....	7
Figure 4. Geologic map (1:300 scale) of the south borrow pit fault at locations 1 and 2 (plate 2).....	12
Figure 5. Sketch geologic map (1:24 scale) showing internal structures between two splays of the south borrow pit fault at location 2 (plate 2).....	13

	<u>Page</u>
Figure 6. Geologic map (1:240 approx. scale) and cross sections showing structural relationships at location 4 (plate 2) where fault A terminates against the south borrow pit fault.....	14
Figure 7. Fracture trace map (1:96 scale) and lower hemisphere equal-area projections of south borrow pit fault, bedding, and fracture data from location 4 (plate 2).....	15
Figure 8. Geologic block diagram (1:12 approx. scale) showing vertical and horizontal sections of fault B where it was excavated in a gully at location 5 (plate 2).....	17
Figure 9. Geologic sketch diagram (1:24 approx. scale) of structural features related to fault C in a scraped and cleaned ditch outcrop of completely decomposed rock at location 8 in the north borrow pit (plate 1).....	17
Figure 10. Photograph of fracture patterns in rocks in a completely decomposed outcrop about 100 feet south of the surface trace of the south borrow pit fault at location 6 (plate 2).....	19
Figure 11. Rose diagrams and lower hemisphere equal-area stereonet projections of structural data from the north and south borrow pits.....	21
Figure 12. Detailed geologic map (1:15 scale) and lower hemisphere equal area projections of structures in the footwall of the south borrow pit fault at location 4 (plate 2).....	22
Figure 13. Schematic diagram showing a possible kinematic model for the south borrow pit fault and associated structures.....	27

TABLES

Table 1. Summary table of fracture properties for the fracture trace map area in the hanging wall of the the south borrow pit fault shown in figure 7 (location 4, plate 2).....	24
Table 2. Table relating structures, primary fracture sets, and tectonic processes for the those features in the study area whose relative ages could be determined from field relationships.....	25
Table 3. Table summarizing the Unified Rock Classification System.....	46

PLATES

Plate 1. Bedrock geologic map of the north and south borrow pits (1:3,750 approx. scale).....	in pocket
Plate 2. Bedrock geologic map of the south borrow pit (1:2,145 approx. scale).....	in pocket

Bedrock Geologic Maps, and Fracture and Fault Data for Portions of the Cokesbury and New Hill 7.5-Minute Quadrangles, Deep River Triassic Basin, Wake County, North Carolina

by

Richard M. Wooten, Timothy W. Clark, and Timothy L. Davis

ABSTRACT

Detailed geologic mapping (1:12 to 1:3,750 scale) and structural investigations were conducted in a well-exposed sequence of Triassic age sedimentary rocks in the New Hill and Cokesbury 7.5-minute quadrangles. The rocks studied are exposed in excavations made in the late-1970's for material to construct the auxiliary dam for the Shearon Harris nuclear power plant. These two areas, informally referred to as the north and south borrow pits, expose a heterogeneous siliciclastic sequence of conglomerate, sandstone, siltstone, and mudstone characteristic of the Deep River Triassic basin.

Geologic mapping in the study area reveals stratigraphic marker units, map- and outcrop-scale folding, and four previously unreported faults. Stratigraphic marker units can be traced along strike for up to several hundreds of feet. The main fault, informally referred to here as the south borrow pit fault (SBPF), has a generalized strike of N. 72° W. with a 30° to 70° southwest dip, and has a minimum trace length of 1,400 feet across the south borrow pit. The total displacements along the SBPF and the other faults reported here are not determinable from available data. Two dominant fracture sets occur in the study area: 1) a set striking generally parallel to the SBPF, and 2) a set striking generally north at a high angle to the SBPF.

Kinematic studies suggest two stages of displacement in the study area: 1) normal faulting, and 2) normal and dextral strike-slip faulting. The map-scale fold that characterizes the map pattern of the south borrow pit is interpreted as a hanging wall anticline related to normal faulting along the SBPF during stage 2. Two additional faults, exposed approximately 500 feet apart in the south borrow pit, strike oblique to the SBPF. A fourth fault, near the north borrow pit, strikes N. 35° E. and dips 60° S. These four newly discovered faults, along with other faults previously identified in the area, indicate this portion of the Deep River Triassic basin is a structurally complex zone of intersecting faults.

INTRODUCTION

This report presents geologic maps and data collected to date by North

Carolina Geological Survey (NCGS) staff during ongoing geologic investigations of the Deep River Triassic basin (fig. 1). The investigations concentrated on bedrock exposures in two borrow pits west of the Shearon Harris nuclear power plant (fig. 2) near the boundary between the Cokesbury and New Hill 7.5-minute quadrangles, Wake County, North Carolina.

The borrow pits (referred to as the north and south borrow pits) are partly within the proposed Wake/Chatham low-level radioactive waste (LLRW) disposal site and are bounded on the east by the Shearon Harris Reservoir (fig. 2). Excavated in the mid-1970's for clayey soil used to construct the auxiliary dam for the Shearon Harris nuclear power plant, the north and south borrow pits encompass approximately 0.11 and 0.08 square miles (70 and 50 acres) respectively. Although weathered and partly revegetated, the borrow pits contain abundant outcrops allowing detailed geologic mapping.

Geologic mapping (1:2,145 and 1:3,750 scale) in the study area focused on the extent of readily recognizable stratigraphic units and the delineation of major structures and structural trends (plates 1 and 2). During the course of geologic mapping three faults were identified in the south borrow pit and one fault was identified near the north borrow pit. The main fault is referred to here informally as the south borrow pit fault (SBPF) and is the primary focus of the structural analysis in this report. The other faults are informally referred to as faults A, B, and C respectively.

Larger-scale geologic mapping (1:12 to 1:300 scale), data collection, and structural analyses were conducted at locations 1 through 7 on plate 2, and location 8 on plate 1. These detailed studies were conducted along or near these faults to determine fault kinematics and the characteristics of fractures and other fault-related structures.

The results of this investigation contribute to two ongoing projects by the NCGS: 1) 1:100,000-scale geologic mapping in the Raleigh 30 x 60-minute quadrangle; and, 2) independent data collection and evaluation related to regulatory oversight of geologically related sections of the Safety Analysis Report for the proposed Wake/Chatham low-level radioactive waste (LLRW) disposal site prepared by Chem-Nuclear Systems, Inc. (1993). The information contained in this report is preliminary, but it is being released since it is relevant to geologic studies of the proposed Wake/Chatham LLRW site.

REGIONAL OVERVIEW

The Deep River Triassic basin is the southernmost exposed rift basin of Triassic age in eastern North America. This basin is composed of three connected basins. From north to south these are the Durham, Sanford, and Wadesboro Triassic basins (fig. 1).

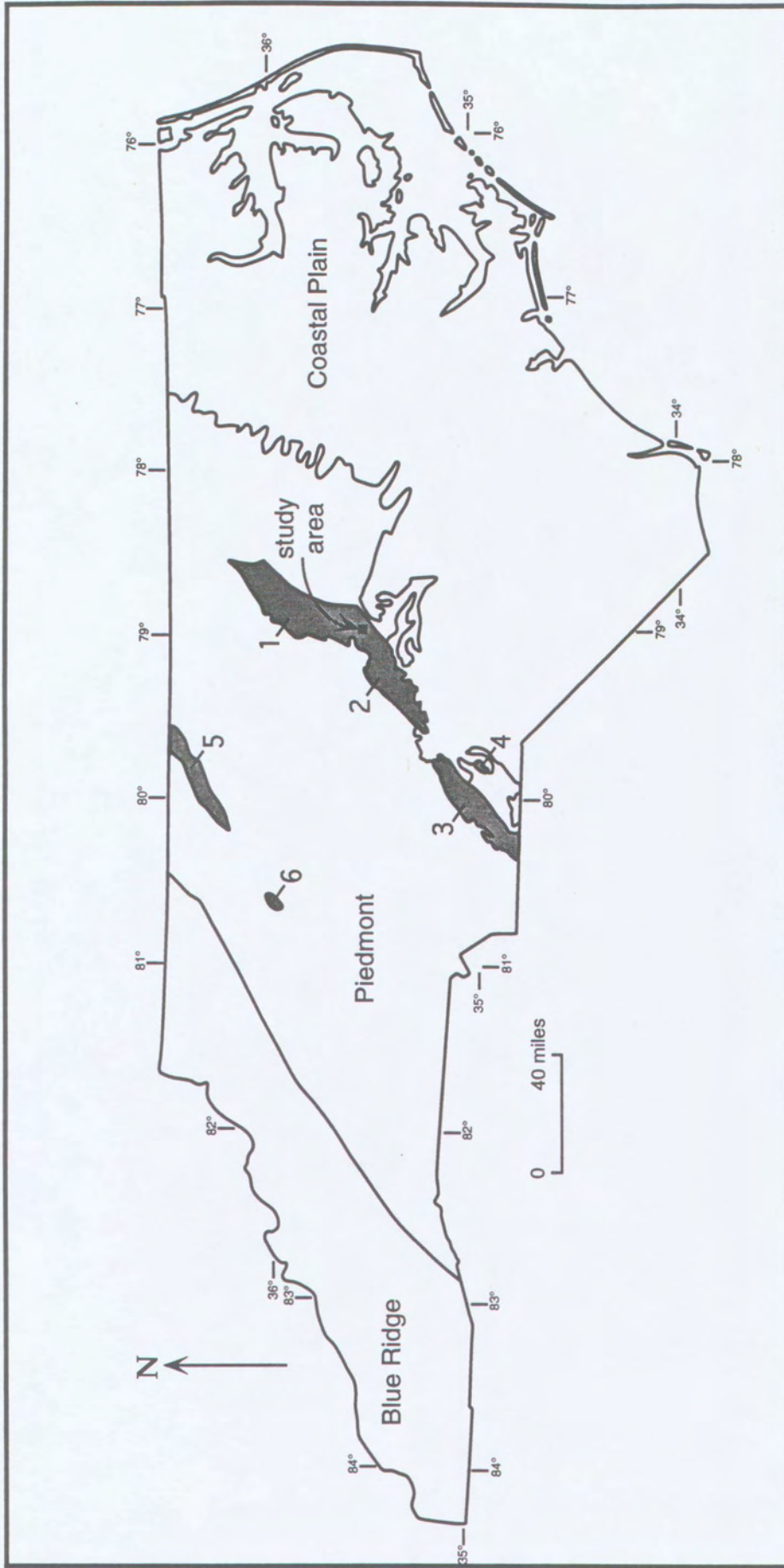


Figure 1. Physiographic provinces and Triassic rift basins (shaded) of North Carolina in relationship to study area. Key: 1, 2, and 3 - Deep River basin (1 - Durham basin, 2 - Sanford basin, 3 - Wadesboro basin); 4 - Dan River basin; 5 - Ellerbe basin; 6 - Davie County basin.

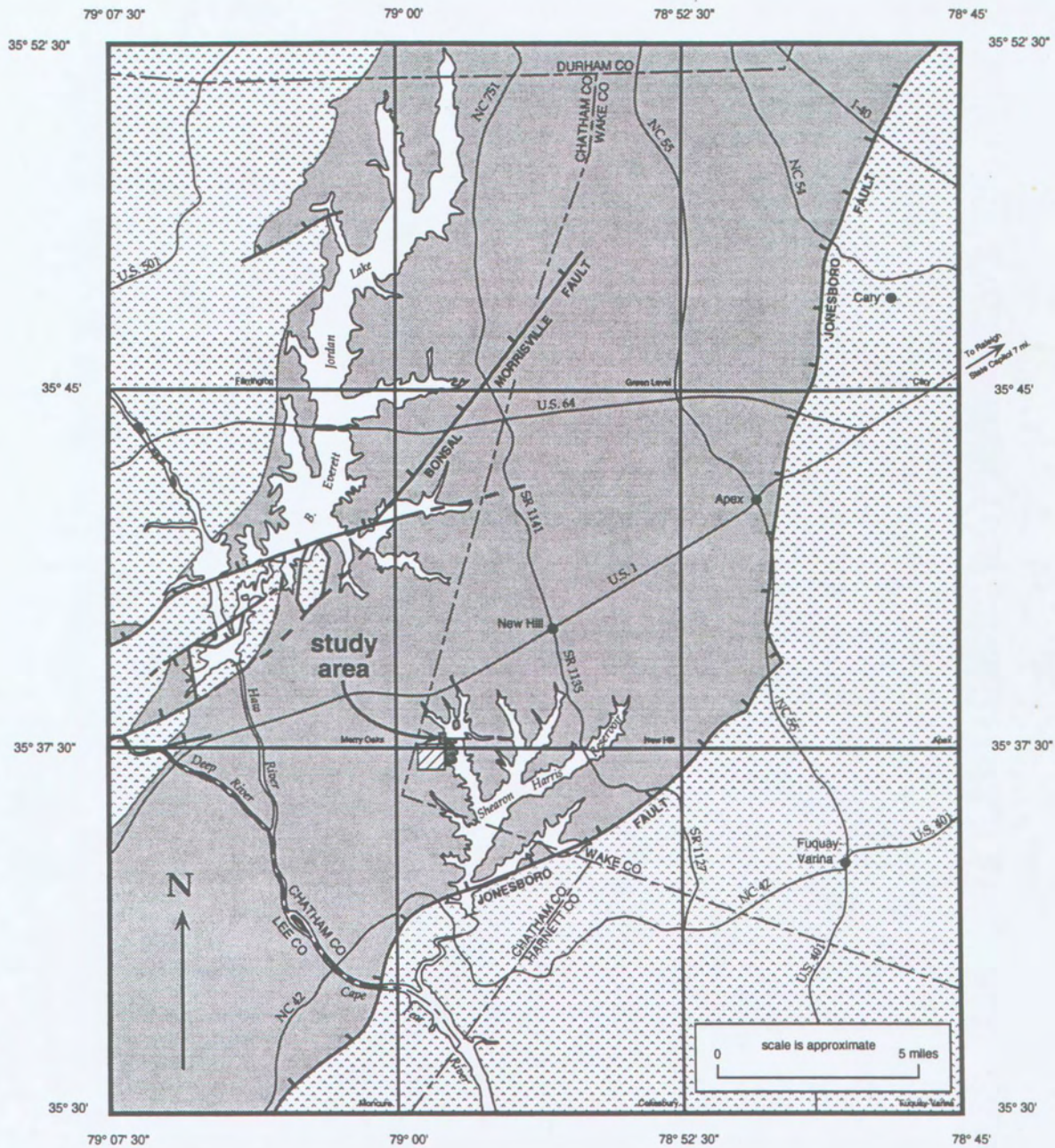


Figure 2. Generalized geologic map (post-Triassic units not shown) of the southern Durham basin with study area and 7.5-minute quadrangles outlined (modified after North Carolina Geological Survey, 1985). USGS 7.5-minute quadrangle names are shown in lower right corner of each quadrangle.

Rocks of the Deep River Triassic basin are included in the Chatham Group of the Newark Supergroup (Olsen, 1978; Luttrell, 1989; and Olsen and others, 1991). Campbell and Kimball (1923) subdivided the Chatham Group in the Sanford Triassic basin into the Pekin, Cumnock, and Sanford Formations, and their extent was later refined by Reinemund (1955). These formal stratigraphic names are restricted to the Sanford Triassic basin. No formal formations are recognized in the Durham basin; however, several subdivisions are made from lithofacies mapping (Bain and Harvey, 1977; Wheeler and Textoris, 1978; Gore, 1986; Hoffman and Gallagher, 1989). The Chatham Group consists of conglomerate, sandstone, siltstone, claystone, shale, coal (Sanford Basin only), and small amounts of limestone and chert (Durham Basin only) formed in lacustrine, fluvial, and alluvial fan depositional systems (e.g., Hoffman and Gallagher, 1989 and Olsen and others, 1991).

The Deep River basin is a north-northeast trending half-graben, bordered on the east by the Jonesboro fault, a west-dipping, stepped, high-angle normal fault (Bain and Brown, 1980; Olsen and others, 1991). Along the western margin, sedimentary rocks unconformably overlie Late Proterozoic and Cambrian metavolcanic and metasedimentary rocks of the Carolina slate belt (North Carolina Geological Survey, 1985). Faults also form the basin boundary locally along its western border. Sedimentary rocks in the Durham basin generally dip toward the east to a maximum thickness of approximately 6,000 to 7,000 feet (Parker, 1979).

Triassic sedimentary rocks throughout the Deep River Basin are intruded by Early Jurassic diabase dikes and sills. Locally, both Triassic and Jurassic rocks are unconformably overlain by Cretaceous deposits and fossiliferous Eocene outliers of the Atlantic Coastal Plain and Tertiary upland gravels (North Carolina Geological Survey, 1985).

The Durham and Sanford basins are separated by a narrower segment of the Deep River basin commonly referred to as the Colon cross-structure. This narrower segment contains map-scale faults, folds, and clusters of diabase dikes, and is interpreted as a basement high between the Sanford and Durham basins (Campbell and Kimball, 1923, Reinemund, 1955). Further studies are necessary to determine the extent, structural components, and evolution of the Colon cross-structure. The study area lies in the transition between the southern end of Durham basin and the northern extent of the Colon cross-structure (figs. 1 and 2).

Bain and Harvey (1977) and Bain and Brown (1980) conducted regional geologic mapping and fault investigations in the Durham Triassic basin north of the Colon cross-structure. In their model, northeast-trending faults and fracture zones are cross-faulted along north-northwest-trending faults and fracture zones to produce diamond and triangular shaped fault blocks in map view. Additional information on the geology of the Deep River Triassic basin can be found in Parker (1979), Textoris and Robbins (1988), Huber and others (1993), Hu and Textoris (1994), and Textoris and Gore (1994).

PREVIOUS AND ONGOING STUDIES

A detailed geologic investigation in the vicinity of the study area was conducted in the early to mid-1970's to support the site characterization and construction of the Shearon Harris nuclear power plant. The Harris fault (plate 1) was identified during excavation for the plant, and was the subject of geologic mapping (1:7,200 scale) of specifically scraped and trenched areas. This geologic information is included in an unpublished report by Ebasco Services, Inc. (1975). Arbogast (1976) studied exposures in the foundation excavations for the Shearon Harris power plant during his geologic investigation of the area.

The Harris fault is now concealed beneath the Shearon Harris nuclear power plant and the Shearon Harris Reservoir. The Harris fault strikes generally east-northeast and dips steeply to the south. It has a known trace length of nearly 3,000 feet extending from the power plant as far west as the auxiliary dam on the Shearon Harris Reservoir (plate 1 and figure 3). A minimum age of 150 million years for the Harris fault, and evidence for both normal (down-to-the-south) and left-lateral, strike-slip displacement were reported by Ebasco Services, Inc. (1975).

Chem-Nuclear Systems, Inc. has conducted geologic investigations at the proposed Wake/Chatham LLRW site beginning in 1991 (Chem-Nuclear Systems, Inc., 1993). Two faults, informally referred to as the W8 and W82 faults, were identified during characterization of the Wake/Chatham site, and are located approximately 1,000-1,500 feet west of the study area. The confirmed segment of the W8 fault strikes north-northeast and dips towards the west; the confirmed segment of the W82 fault strikes east-northeast (subparallel to the Harris fault) and dips toward the south. Chem-Nuclear Systems, Inc. (1993) interpreted the W8 and W82 faults to be normal faults, and the Harris, W8, and W82 faults to be part of a sinistral Riedel shear system. The east-northeast strike of the W82 fault indicates it may project from its easternmost known location (approximately 1,000 feet west of the study area) into the southern part of the south borrow pit. NCGS mapping to date, however, has not located this fault in the south borrow pit.

Discussions of investigations of the W8 and W82 faults and other geologic aspects of the proposed Wake/Chatham LLRW site are contained in the Safety Analysis Report for the Wake/Chatham site (Chem-Nuclear Systems, Inc., 1993). Further information on these and possibly other faults may result from future investigations at the Wake/Chatham site.

METHODS

The base maps for the geologic maps of the north and the south borrow pits (plates 1 and 2) are photocopy enlargements of portions of a 1:6,000-scale (approximate) color aerial photograph. This photograph was produced by enlarging a 1:24,750-scale (approximate) photograph taken by Heart of Carolina Aerial

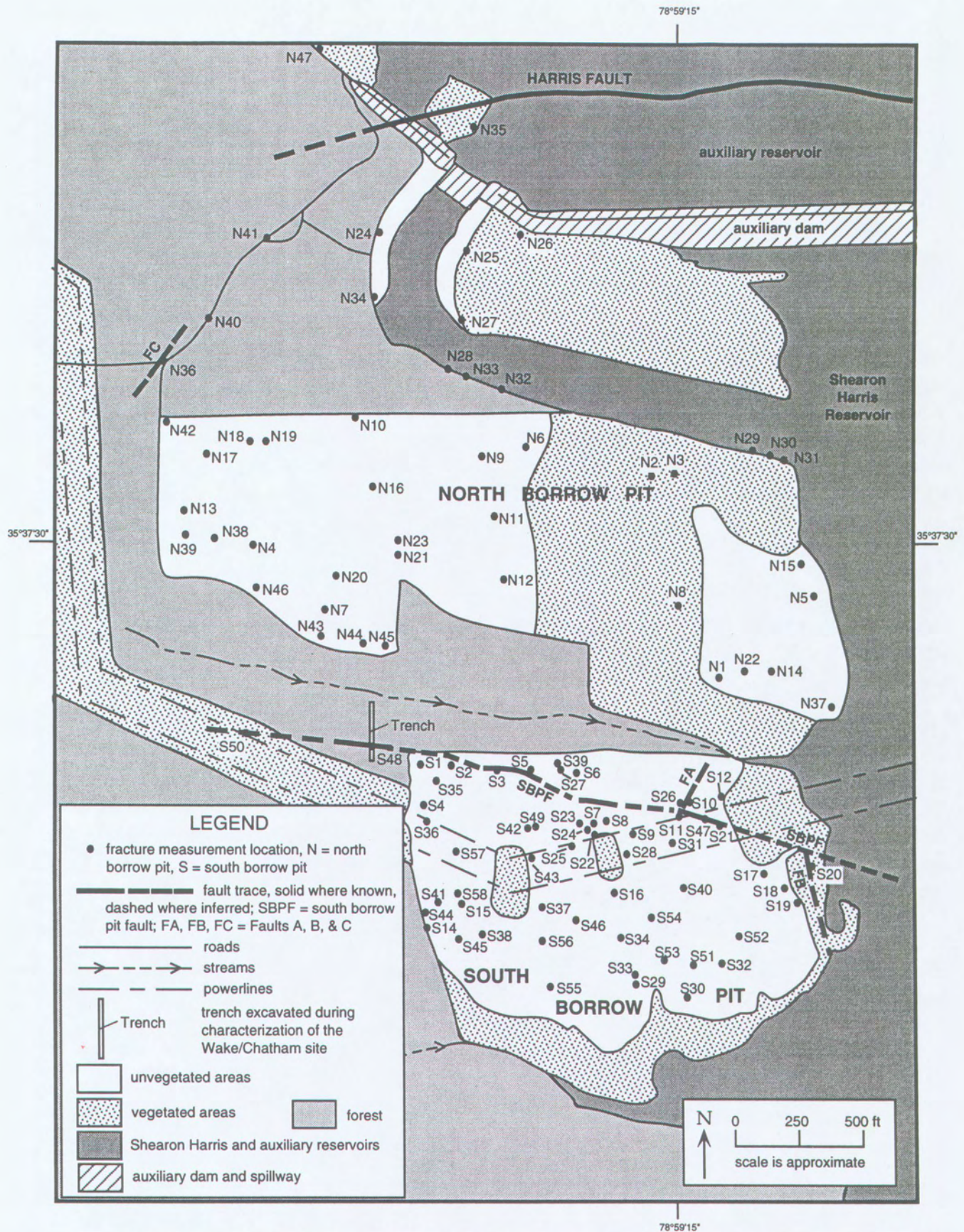


Figure 3. Data location map of the north and south borrow pits showing the distribution of bedding, fault, and fracture measurements. Data is listed in Appendix A.

Surveys, Inc. on October 28, 1989. The scale of the original aerial photograph varies slightly because of differences in the distance between the camera and the ground surface. Additional distortion of scale may have been introduced into the photocopies during the enlargement process; therefore, the scales of the resulting geologic maps shown in plate 1 (1:3,750 scale) and plate 2 (1: 2,145 scale) are also only approximate. Despite the small variations in scale, the color aerial photograph was a useful base map because: 1) outcrops could readily be located in the field; 2) color differences in the unvegetated areas aided in the recognition of lithologic units; and, 3) their relatively large scale permitted detailed geologic mapping.

Geologic mapping (data collection and compilation) was conducted by standard techniques (e.g., Compton, 1962). Geologic data were collected from outcrops and shallow, hand-dug test pits. Scraping and sweeping of weathered rock outcrops was needed in many cases to expose the relevant geologic features. A leaf blower was used to remove loose material from some of the scraped outcrops. Bedding, tectonic fracture, and fault orientation data were collected from 96 stations in the borrow pits and near the auxiliary dam spillway (fig. 3) using a Brunton compass. These data are presented in tabular form in Appendices A and B. Fractures considered to be tectonic include those that: 1) have generally planar surfaces; 2) occur in sets; 3) have local or regionally consistent orientations; or, 4) have surface markings indicative of tectonic origin. Structural data were plotted on lower hemisphere, equal-area projections and rose diagrams using a computer code developed by Allmendinger (1995).

The Unified Rock Classification System (URCS), developed by Williamson (1984), was applied at the reconnaissance level to supplement standard geologic classifications with information on the basic engineering properties of the weathered rocks exposed in the borrow pits. The terminology used in the body of this report to describe the weathering state of rock conforms to the URCS. Refer to Appendix C for text and information on the engineering rock mass classification used in this study.

The 1:300-scale map (fig. 4) for locations 1 and 2 (plate 2) along the SBPF was constructed by surveying a baseline with a Brunton compass, a hand-held clinometer, and a 100-foot cloth tape. Locations of the outcrops and test pits used to construct this map were referenced to the baseline by pacing or measuring distances with a tape. The 1:240-scale map for location 4 (plate 2) shown in figure 6 was constructed using a Brunton compass, a hand-held clinometer, and a 100-foot cloth tape to locate outcrops relative to a ground reference point established for the fracture trace map shown in figure 7.

Fracture trace mapping at a scale of 1:12 was conducted over an area of approximately 500 square feet at location 4 (plate 2) using a grid separated into 1-foot-square cells. This mapping is presented as the 1:96-scale map in figure 7. Along and immediately adjacent to the SBPF, a 20-foot by 20-foot semi-permanent grid

(i.e., nails and nylon string) oriented north-to-south by a hand-held Brunton compass was used to facilitate fracture mapping. Elsewhere, a portable 4-foot by 4-foot grid constructed of 5/8 inch polyvinyl-chloride pipe and nylon string was used. The portable grid was oriented using a north-to-south baseline extended from the fixed grid area. The portable grid was also used to construct the fracture trace map for figure 12. The traces of all fractures interpreted as tectonic in origin were mapped in each of the grid cells. Orientation data for each of the 300 fractures measured at this location are included in Appendix B and plotted on lower hemisphere, equal-area projections shown in figure 7.

English units of measurement are used to facilitate relating the data contained in this report with data in the Safety Analysis Report prepared by Chem-Nuclear Systems, Inc. (1993) for the proposed Wake/Chatham LLRW disposal site.

GENERAL STRATIGRAPHY

Exposed in the north and south borrow pits is a heterogeneous, siliciclastic sequence of conglomeratic sandstone, muddy sandstone, siltstone, and mudstone (classified according to Folk 1974, 1980). Basic lithologic descriptions of the mapped rock units are included on the geologic maps (plates 1 and 2).

Geologic mapping in the borrow pits focused on the extent of readily recognizable stratigraphic markers. Conglomeratic sandstone, sandstone, and purple mudstone and siltstone were the three key marker units mapped (plates 1 and 2). In several cases, these marker units were traced for several hundreds of feet. Preliminary stratigraphic analysis of rock units in the study area indicates the thickness of individual stratigraphic units ranges from a few feet to tens of feet. Further studies are necessary to describe the sedimentary features and the stratigraphic aspects of the exposed sequence of rock in more detail.

STRUCTURE

BEDDING ORIENTATION

Geologic mapping of stratigraphic marker units described above resulted in defining a contrast in structural patterns between the north and south borrow pits (plates 1 and 2). Rock units in the north borrow pit generally strike north-northwest with a gentle (approximately 8° to 25°) east-northeast dip. A small number of exposures show a localized northeast strike of rock units near a northeast-striking fault (referred to as fault C in this report) exposed along the access road to the north borrow pit (location 8, plate 1 and fig. 9). Although map data are limited, significant deflections in the orientation of stratigraphic marker units have not been observed in the north borrow pit near the Harris fault (plate 1).

Geologic mapping in the south borrow pit revealed marked variation in the

strike of rock units, which led to the discovery of the SBPF (plates 1 and 2). The change in orientation of rock units in the south borrow pit can be observed on a traverse from south to north toward the SBPF. This change in strike is discernible on aerial photographs as curved, discontinuous, light-colored bands marking completely decomposed mudstones and siltstones exposed in unvegetated parts of the south borrow pit (plates 1 and 2).

In the southernmost portion of the south borrow pit, rock units generally strike north to north-northeast and dip gently east. Approximately 450 to 600 feet (map distance) south of the SBPF, the strike of the rock units changes to the northwest and dip direction changes to the northeast. This northwest strike of rocks persists to within 35 to 50 feet of the SBPF, where locally the strike changes to the north-northeast. These changes in the orientation of rock units delineate fault-related, map-scale anticlinal folding and outcrop-scale synclinal folding in the hanging wall of the SBPF. These folds are interpreted to be longitudinal folds subparallel to the associated fault as discussed in Schlische (1995).

Geologic mapping also indicates that immediately north of the SBPF, bedding strike changes from northeast to northwest near the drainage separating the borrow pits (plate 1 and fig. 3). This change suggests the possibility of additional faulting and fault-related folding (i.e., an east-plunging anticline) in the vegetated area between the borrow pits. The general strike of the SBPF parallels the trend of the drainage separating the north and south borrow pits suggesting a possible structural control on the drainage.

FAULTS

South Borrow Pit Fault

The SBPF was identified at several exposures in the south borrow pit (locations 1, 2, 3, 4 and 7, plate 2). The generalized strike of the SBPF is N. 72° W. with dips ranging from 30°-70° S. The SBPF has a minimum trace length of approximately 1,400 feet based on known exposures and exhibits a "right-stepping" pattern across the south borrow pit with hanging wall (south side) and footwall (north side) components. The general west-northwest strike of the SBPF contrasts with the general east-northeast strike of the Harris fault.

Larger-scale geologic mapping (1:300 scale) at the westernmost exposure of the SBPF in the south borrow pit (locations 1 and 2, plate 2 and fig. 4) shows the orientation of the fault's map trace varies from N. 80° E. to N. 50° W. over a strike distance of about 200 feet. The dip of the fault plane ranges from 40° S. to vertical in this area. Figure 4 also illustrates the truncation of map units by the SBPF, and outcrop-scale synclinal folding on the hanging wall (south) side of the SBPF similar to that observed at location 4 (plate 2) and shown in figures 6 and 7.

Geologic mapping (1:24 scale) shown in figure 5 (location 2, plate 2) illustrates structures between two splays of the SBPF comprised of clayey gouge and breccia. Between these two splays, lithologic contacts and associated fractures are deformed into sigmoidal shapes resembling those expected in a Riedel shear model (inset diagram, fig. 5). Sigmoidal sandstone bodies with the same sense of asymmetry were also observed at locations 4 and 7 (plate 2).

Rocks in the SBPF exhibit fabrics characteristic of fault rock produced during brittle to semi-brittle faulting as described by Sibson (1977) and McClay (1987). These fabrics in the SBPF fault rocks include breccia, foliated breccia and clayey gouge. Random-fabric breccias with clasts up to 2.5 feet in length are derived from clast-supported rocks, whereas foliated breccias containing numerous hand specimen-scale slip surfaces are more typical in matrix-supported rocks. clayey gouge ranges in color from red-brown to tan to pale gray. Breccias are typically red to red-brown. Black to dark gray oxide staining on fractures and mineral grains commonly occurs in rocks adjacent to the fault.

Fault A

Fault A is a northeast-striking fault with a nearly vertical to steep easterly dip that crops out in the south borrow pit at location 4 (plate 2). The southern end of this fault terminates against the SBPF (fig. 6) and the northern end is covered by recent slope wash deposits. Evidence for fault A has not been identified in the north borrow pit, or elsewhere in the south borrow pit. Figure 6 shows a geologic map and cross sections of field relationships at location 4.

Fault A is characterized by partially to completely decomposed foliated breccia, random-fabric breccia and contorted beds. Foliated mudstone and siltstone breccia with local discontinuous sandstone lenses and blocks are the predominate fault zone rocks. Aligned blocks and lens-shaped bodies of sandstone and siltstone within the foliated mudstone breccia locally define intervals of compositional layering. The interval of contorted bedding and brecciated rock comprising the fault zone ranges in width from 3 to 10 feet and can be traced for approximately 110 feet along strike. Small scale folds with curved axial planes and northeast plunging fold axes occur within the fault zone. These folds are typically truncated by offsets within the fault zone (inset C, fig. 6).

Small-scale folds and contorted beds also occur along both the northwest and southeast margins of fault A. Drag folding (cross sections X-X' and Y-Y', fig. 6) indicates a component of normal displacement (down to the southeast). The strike of the foliation and compositional layering within the fault zone is generally oblique to the strike of the fault in map view. This angular relationship and the northeast-trending folds within the fault zone suggest a dextral strike-slip component of displacement, possibly associated with reactivation of fault A during movement along the SBPF. The amount of displacement along fault A has not

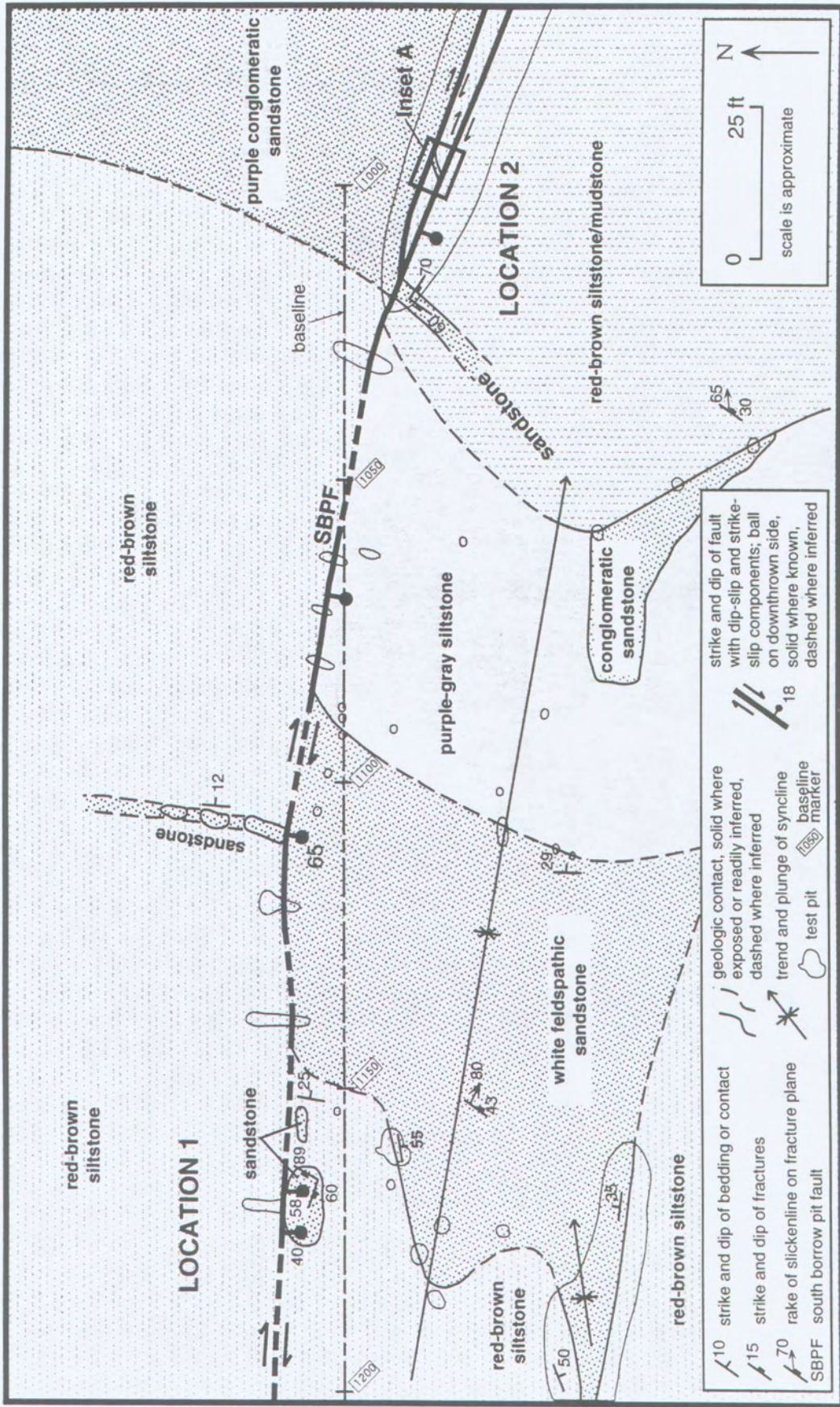


Figure 4. Geologic outcrop map (1:300 approx. scale) of the south borrow pit fault (SBPF) at locations 1 and 2 (plate 2). Inset A - map area for figure 5.

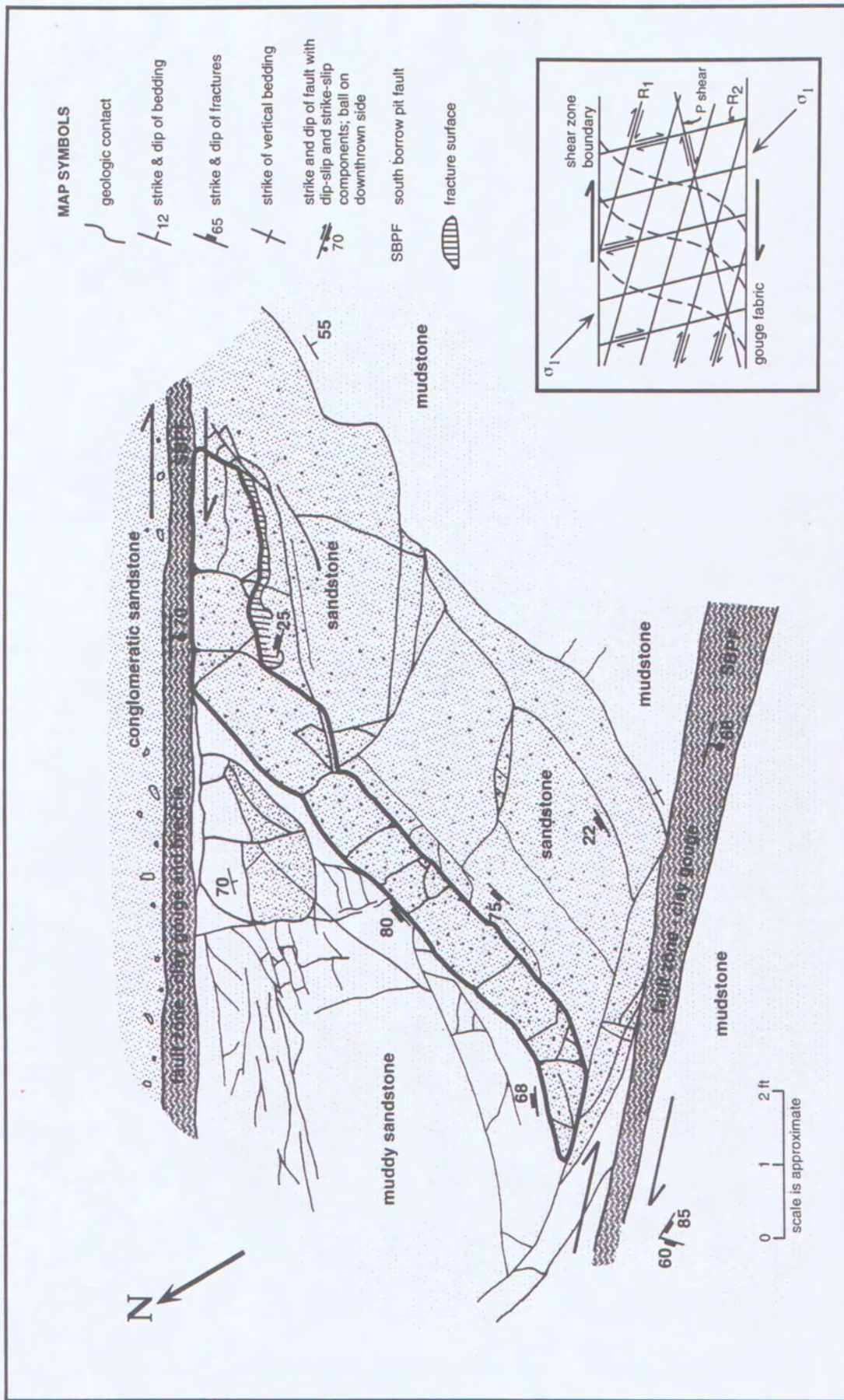


Figure 5. Geologic map (1:24 scale) showing internal structures between two splays of the south borrow pit fault (SBPF) exposed at location 2 (plate 2). Deformed and truncated beds occur between two fault splays defined by clay gouge, breccia, and foliated breccia. The sigmoidal shape of the lithologic contacts and associated fractures (bold lines) between the splays indicates a dextral sense of shear consistent with the Riedel shear model shown in the inset diagram (inset modified from McClay (1987)). Fault splays converge to the northwest (see figure 4).

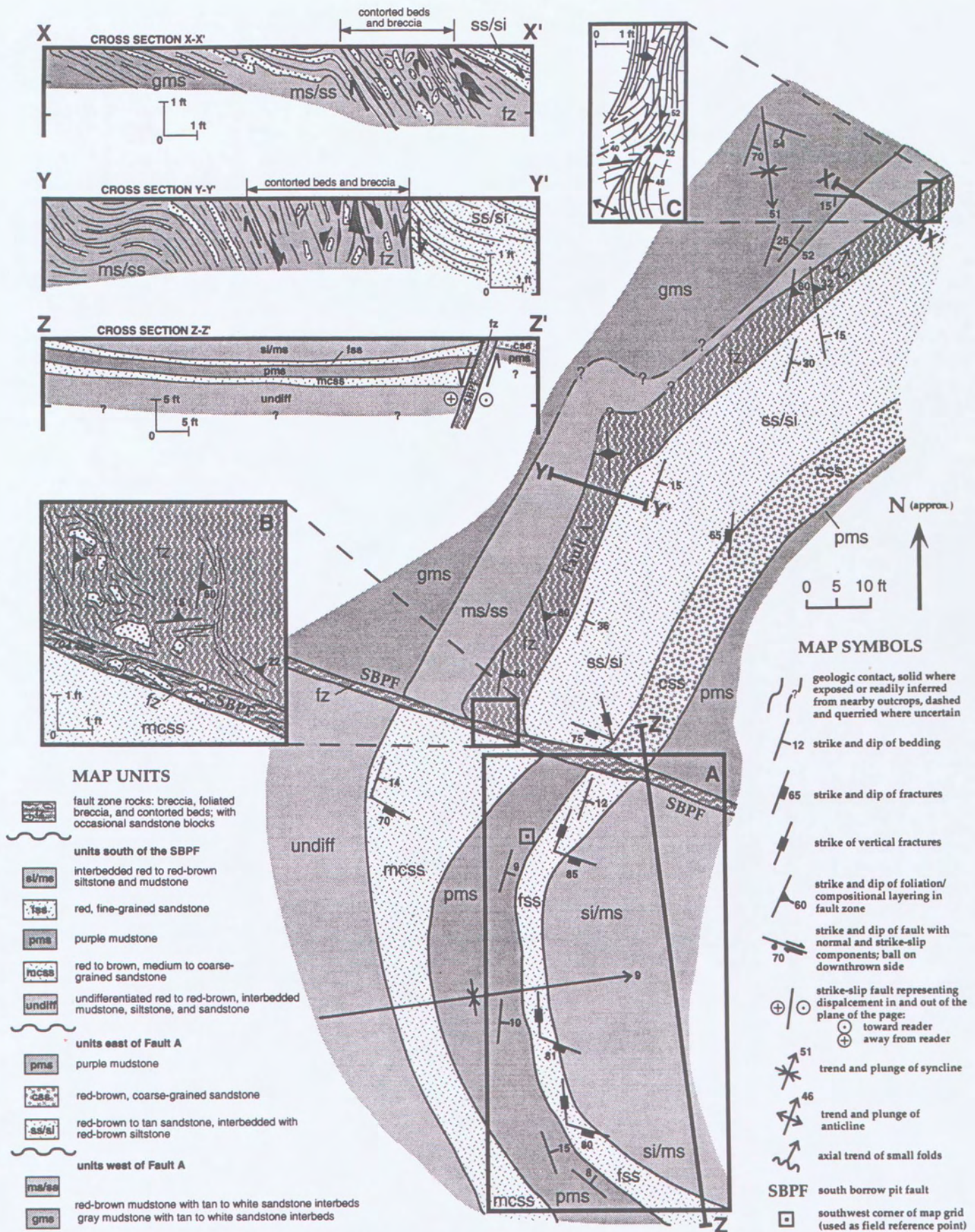


Figure 6. Geologic map (1:240 scale) and cross sections showing structural relationships at location 4 (plate 2) where fault A terminates against the south borrow pit fault (SBPF). Inset A - fracture trace map area for figure 7. Inset B - detail of the fault fabric where fault A terminates against the SBPF. Inset C - schematic detail of deformation patterns within fault A.

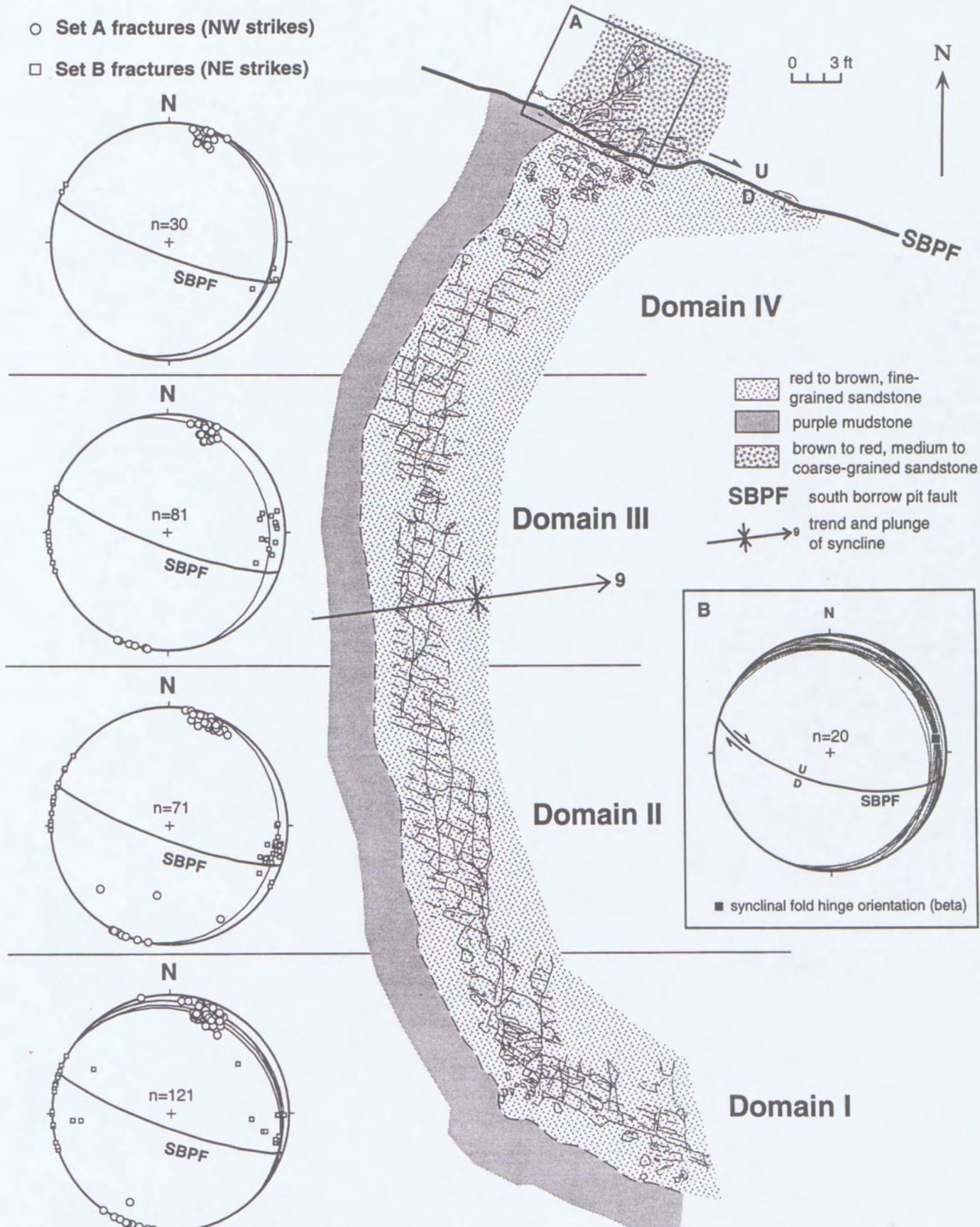


Figure 7. Fracture trace map (1:96 scale) and lower hemisphere equal-area projections of the south borrow pit fault (SBPF), bedding, and fracture data from location 4 (plate 2). Map area is divided into domains I, II, III, and IV based on changes in bedding strike. Projections include: fault and bedding orientations (great circles) and fractures (poles to planes); Set A fractures (filled circles); and Set B fractures (filled squares). Data for projections are listed in Appendix B. Inset A - map area for figure 12. Inset B - lower hemisphere equal area projection of bedding and fault orientations (great circles) and synclinal fold hinge orientation (beta) from the detailed fracture trace map area.

been determined. The termination of fault A against the SBPF indicates the main displacement along fault A occurred prior to displacement along the SBPF.

Fault B

Fault B crops out in a gully near the shore of Shearon Harris Reservoir at location 5 (plate 2) in the south borrow pit. Fault B strikes N. 20°-25°W. and dips 85°-90° W. and can be traced in outcrop about 80 feet along strike. The intersection of fault B with the SBPF is not exposed; therefore, relative age relationships between the faults could not be determined. Figure 8 shows a sketch of fault B exposed in a scraped and cleaned gully outcrop.

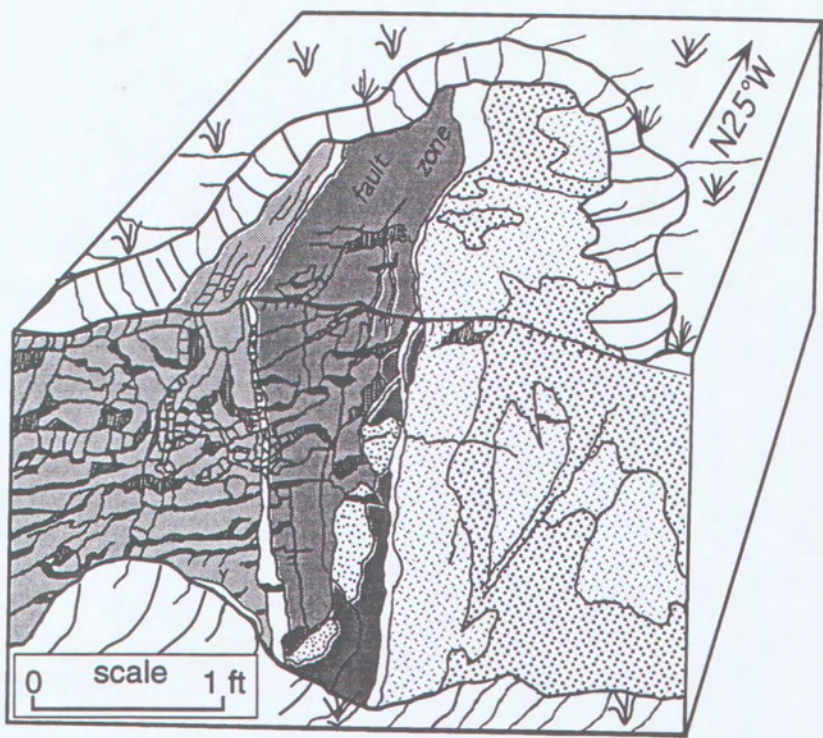
Fault B is marked by the contact between a completely decomposed, tan, fine-grained sandstone with purple mottling in the footwall (east) side of the fault, with a sequence of partially to completely decomposed, red to red-brown, and purple mottled sandstones and mudstones in hanging wall (west) side of the fault. Foliated mudstone breccia and breccia (sandstone clasts in a mudstone matrix) characterize the fault zone and are less than 8 inches thick.

Rocks adjacent to and within the fault are intensely fractured with a fracture spacing generally less than 2 inches. Numerous high-angle fractures subparallel the strike of the fault and contain a white clayey infilling. Northwest-striking fracture sets subparallel to fault B also occur in borrow pit outcrops immediately southwest of location 5 (plate 2). Unequivocal kinematic indicators such as slip surface markings, drag folds or other folds were not observed in the vicinity of fault B. Fault B is interpreted as a normal fault (down to the southwest) given no direct evidence to the contrary, and the generally accepted extensional setting for the Deep River Triassic basin.

Fault C

Fault C is exposed in a ditch outcrop of completely decomposed rock along the access road to the north borrow pit (location 8, plate 1). The fault zone is a 10-13 inch wide foliated breccia with gravel-sized clasts in a foliated mudstone matrix. This interval is distinguished by thin (<2 inch thick), alternating red, tan, and gray color bands. The fault has a generalized strike and dip of N. 35°E. 60°S. Figure 9 shows a schematic geologic sketch map depicting the structural features in the outcrop at location 8 (plate 1).

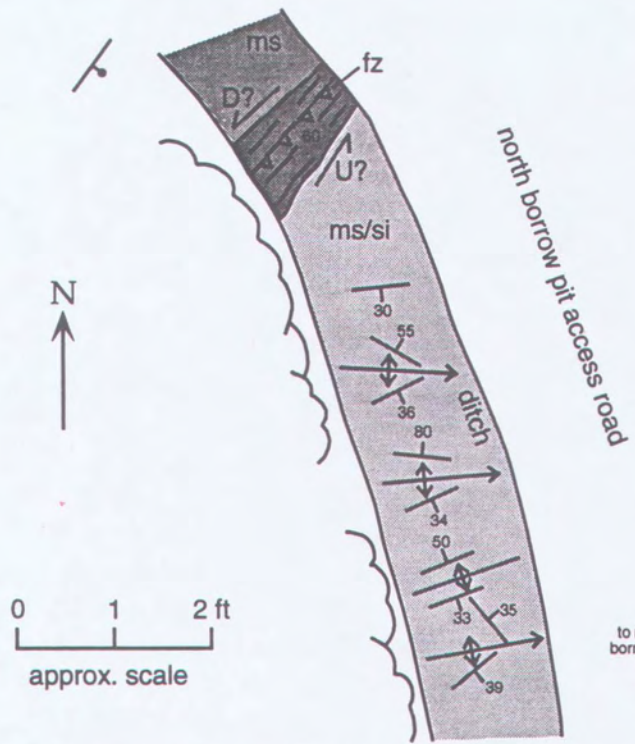
Several outcrop-scale folds within a red-brown mudstone with tan siltstone laminae crop out in the hanging wall (southeast) side of fault C. The fold axes of this series of small-scale anticlines and synclines generally plunge east with axial planes overturned slightly toward the north. These folds are interpreted as contractional features in the hanging wall indicating left-lateral and possibly a reverse component of displacement along fault C.



LEGEND

- Hanging wall**
- red medium-grained sandstone, partially decomposed
- Fault Zone**
- red-brown mudstone and mudstone breccia
 - red fine-grained sandstone clasts
 - purple-gray, foliated mudstone breccia, completely decomposed
 - fracture with white clay infilling
- Footwall**
- tan (t), fine-grained sandstone with purple (p) mottling, completely decomposed (fracturing obscured by weathering)

Figure 8. Geologic block diagram (1:12 approx. scale) showing vertical and horizontal section of fault B where it was excavated in a gully at location 5 (plate 2). The fault zone is characterized by completely decomposed, red-brown to purple-gray mudstone breccia and foliated mudstone breccia, with inclusions of red fine-grained sandstone clasts. The fault zone is bounded by 0.5-2.0 inch wide fractures with white clayey infilling.



LEGEND

- Hanging wall**
- ms red mudstone, completely decomposed
- Fault Zone**
- fz alternating red, tan, and gray foliated breccia, completely decomposed
- Footwall**
- ms/si red-brown mudstone w/ tan siltstone laminae, completely decomposed
 - strike and dip of fault with dip-slip and strike-slip components; ball on hanging wall side
 - strike and dip of bedding
 - trend of anticline
 - trees

Figure 9. Geologic sketch diagram (1:24 approx. scale) of structural features related to fault C in a scaped and cleaned ditch outcrop of completely decomposed rock at location 8 in the north borrow pit (plate 1). The fault zone is a 10-13 inch wide foliated breccia (foliated mudstone matrix with gravel-sized clasts) distinguished by thin (< 2 inch thick) alternating red, tan, and gray color bands. Small scale folds with east-plunging axes occur on the hanging wall (southeast side) of fault C.

Exposures of fault C could not be traced beyond the outcrop at location 8. Bedding strike ranges from northeast to northwest, and bedding dip direction changes from west to east along the access road to the spillway (to the northeast) and along the access road to the north borrow pit (to the south). These variations in the orientation of bedding suggest fault C extends from location 8 (plate 1) along strike to the northeast and southwest. It is possible fault C is related to structures in the area where the W8 fault to the west meets the Harris Fault to the north.

FRACTURES

Fracture investigations included collection of fracture data across the borrow pits and vicinity, and a detailed study of fractures at location 4 (plate 2 and fig. 7) along the SBPF. This section of the report briefly discusses the results of these investigations.

The majority of fracture data collected across the study area provides basic information on the orientation of the dominant fracture sets observed. Investigations of fracture intensity and spacing, crosscutting and termination relationships, modes of fracture development, and relationships to local and regional structures are only briefly discussed here.

General Fracture Characteristics

Both tectonic and non-tectonic fractures occur in most outcrops in the study area. Fractures attributed to tectonism typically are planar, occur in sets, and generally form systematic, rectilinear patterns in plan view (figs. 7 and 10). Fractures attributed to weathering are typically non-systematic and form curving and polygonal patterns.

Throughout the study areas fractures typically have a gray to pale green clayey infilling, or bleached zones parallel to the fracture surfaces. Black manganese oxide, and rust-colored iron oxide staining along fracture surfaces is common.

The orientation of tectonic fractures varies across both borrow areas as can be seen in plates 1 and 2, and rose diagrams and lower hemisphere equal-area projections shown in figure 11c-f. General fracture populations, however, can be discerned from the data. For example, fracture orientation data from the north borrow pit (figs. 11c and 11e) cluster around north-northwest and east-northeast strikes. The east-northeast fractures generally parallel the strike of the Harris fault. North-northwest fractures group along a similar trend as bedding azimuths (compare figs. 11a and 11c). Field observations in the north borrow pit indicate: 1) the spacing between east-northeast-striking fractures generally decreases with proximity to the Harris fault; and 2) north-northwest-striking fractures occur throughout the north borrow pit.



Figure 10. Photograph of fracture patterns in a completely decomposed outcrop ~100 feet south of the surface trace of the south borrow pit fault (SBPF) at location 6 (plate 2). Fractures are highlighted by a white clay infilling and bleached zones. Two fractures sets predominate: Set A oriented $N.80^{\circ}-85^{\circ}W.$ $75^{\circ}-90^{\circ}S.$, sub-parallel to the strike of the SBPF; and Set B oriented $N.10^{\circ}-26^{\circ}E.$ $\sim 90^{\circ}E.$ Termination relationships determined from this photograph for Set A and Set B fractures in 70 cases are: Set A terminates against Set B, $n=32$; Set B terminates against Set A, $n=29$; and, Sets A and B cross or relationships indeterminate, $n=9$. The roughly equal numbers of Set A terminations against Set B as Set B terminations against Set A suggests that here Sets A and B are coeval. The thicker zone of white clay striking NW. across the photograph marks the NE-dipping contact between a conglomeratic sandstone (css) and siltstone (si). Area shown in photograph about 9 feet by 13 feet, Brunton compass for scale.

In the south borrow pit, the orientations of fracture populations are more variable than in the north borrow pit (compare figs. 11c and 11d). Fracture populations in the south borrow pit cluster around north-northeast, northwest and west-northwest azimuths (figs. 11d and 11f). Fracture populations in the south borrow pit generally correspond to similar groupings in bedding azimuths (compare figs. 11b and 11d); however, most northeast-striking beds in the south borrow pit occur on the footwall (north) side of the SBPF. Fracture population also group around similar azimuths as the faults exposed in the south borrow pit (compare figs. 11d and 11f).

North-northeast- and particularly west-northwest-striking fractures are commonly observed in the vicinity of the SBPF. The outcrop shown in figure 10 is located about 100 feet south of the surface trace of the SBPF, and illustrates the general pattern. Here fractures are highlighted by a light gray, clayey infilling as well as bleached zones along the fracture planes. Two fracture sets predominate: 1) a set oriented N. 85° W. 75°-90° S., sub-parallel to the strike of the SBPF; and 2) a set oriented N. 10-26° E. ~90°, at a high angle to the SBPF. Field observations in the south borrow pit also indicate that fractures oriented sub-parallel to the strike of the SBPF generally increase in frequency near the fault.

Fracture Trace Mapping

This section presents the results and discussion of a detailed fracture investigation based on 1:12-scale fracture trace mapping of an exposed bedrock pavement at location 4 (plate 2) along the SBPF (figs. 6 and 7). This mapping focused on structures of the hanging wall rocks of the SBPF in an effort to understand the distribution and characteristics of fractures adjacent to the fault. Fracture trace mapping in the footwall of the SBPF is limited to that shown in figure 12. Fracture trace mapping permits evaluation of fracture orientations as well as their trace lengths, spatial distribution, interconnections, and crosscutting relationships. Fracture trace mapping is an important component in evaluating the geology and hydrology of fractured rock settings (e.g., Barton and others, 1993; La Pointe and Hudson, 1985).

The fracture trace map shown in figure 7 contains three distinct rock units; one rock unit in the footwall and two rock units in the hanging wall. The footwall rock unit is a brown to red, medium- to coarse-grained sandstone. Hanging wall rock units include a purple mudstone overlain by a fine-grained, red to brown, sandstone. Fracture trace mapping and fracture descriptions were restricted to the fine-grained sandstone unit in the hanging wall of the SBPF. The stratigraphic thickness of the fine-grained sandstone is less than 1 foot.

The strike and dip of rock units in the fracture trace map area (figs. 6 and 7) departs from the general map pattern of the southern borrow pit. In the southernmost portion of the pavement, farthest away from the SBPF, the rock units

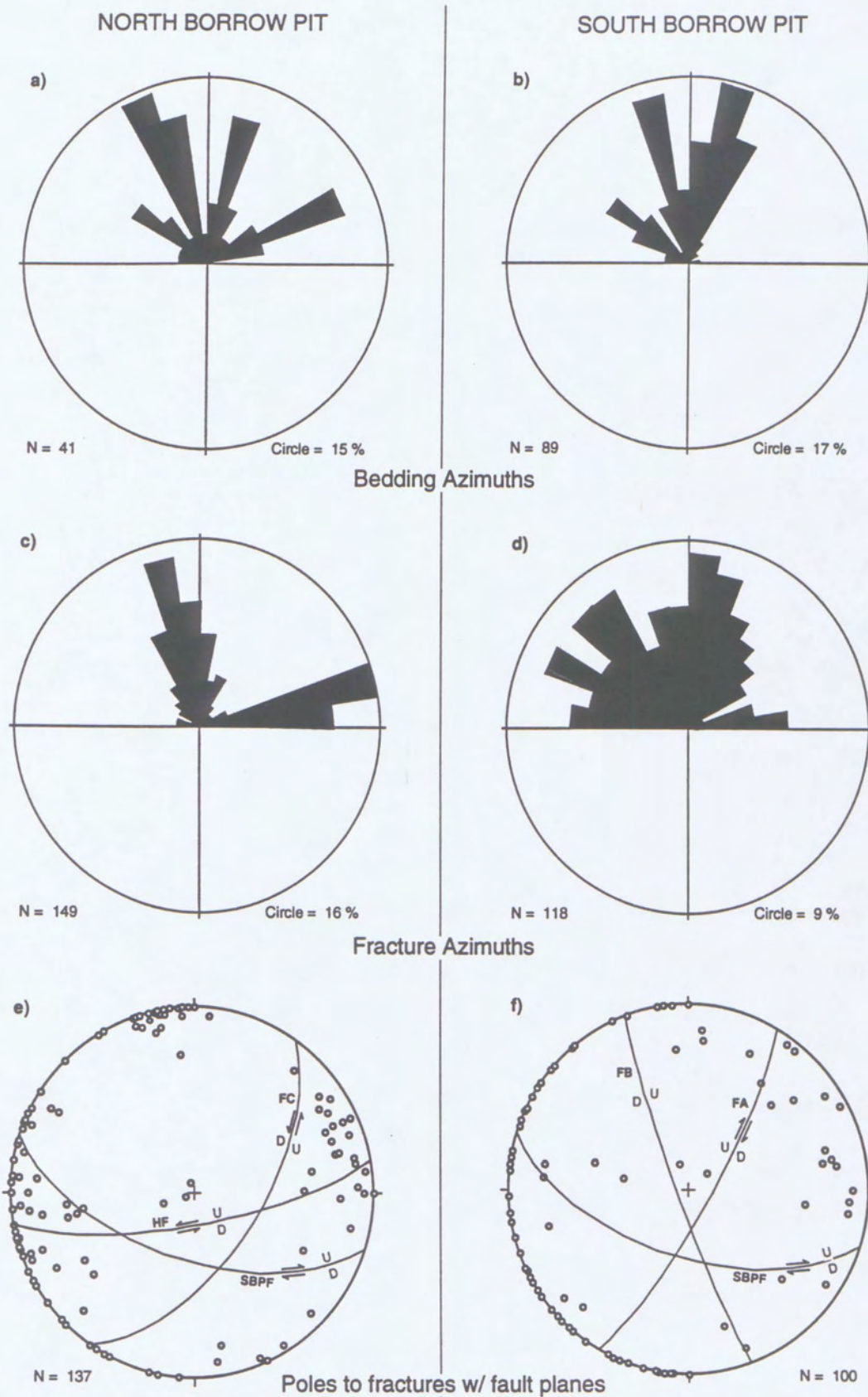


Figure 11. Rose diagrams and lower hemisphere equal-area stereonet projections of structure data from the north and south borrow pits: a) bedding azimuths, north borrow pit; b) bedding azimuths, south borrow pit; c) fracture azimuths, north borrow pit; d) fracture azimuths, south borrow pit; e) fractures (poles) and fault planes (great circle), north borrow pit; f) fractures (poles) and fault planes (great circles), south borrow pit. SBPF = south borrow pit fault; HF = Harris fault; FA = Fault A; FB = Fault B; and FC = Fault C.

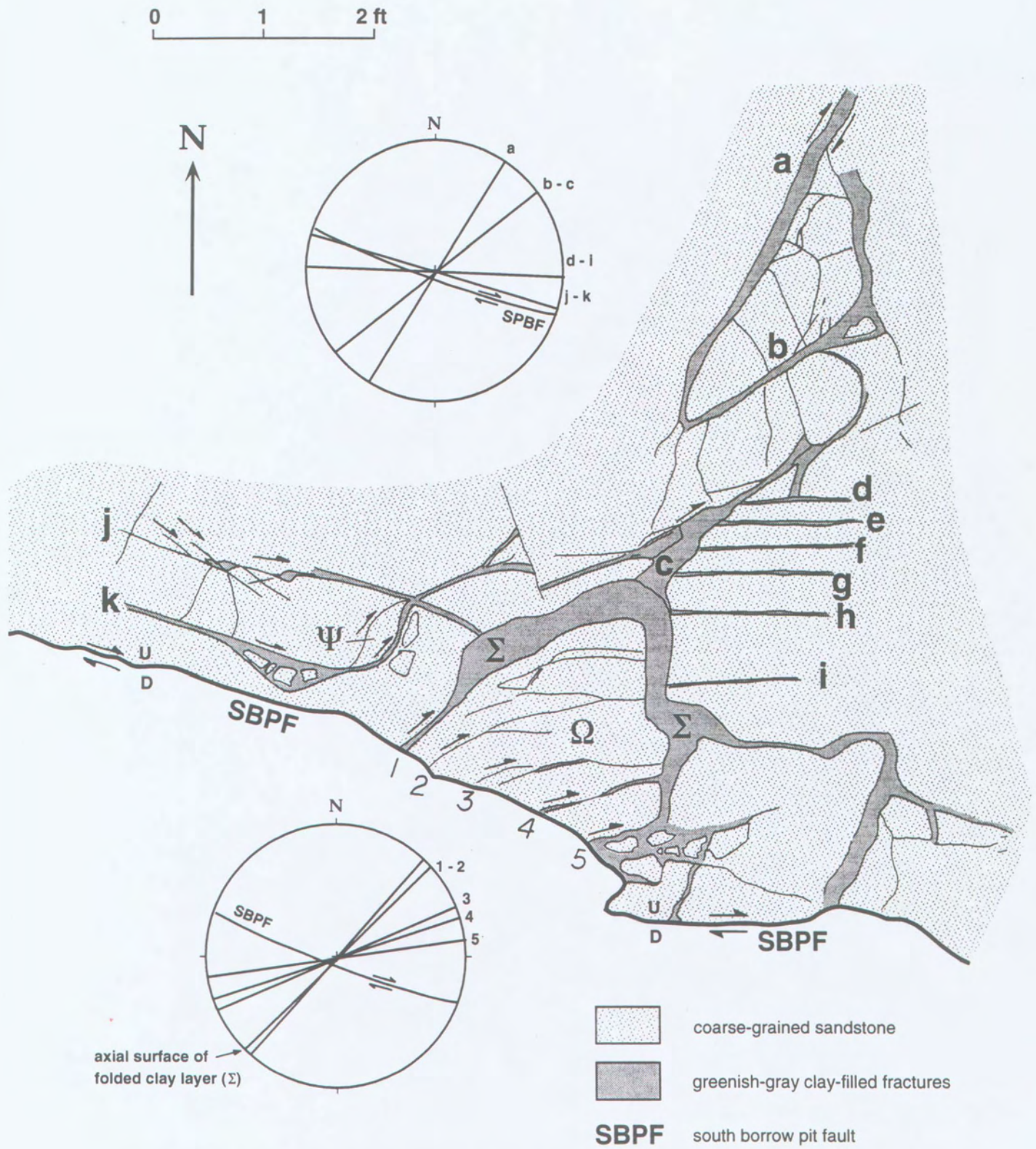


Figure 12. Detailed geologic map (1:15 scale) and lower hemisphere equal area projections of structures in the footwall of the south borrow pit fault at location 4 (plate 2).

strike northwest and dip to the northeast. Near the center of the map area, rocks strike approximately north and dip gently to the east; in the northernmost portion of the pavement, near the SBPF, hanging wall rock units strike northeast and dip gently to the southeast (fig. 7). This change in bedding strike across the map defines an outcrop-scale syncline within the hanging wall of the SBPF. The beta diagram constructed from bedding data defines a fold axis of N. 83° E. 9° (inset B, fig. 7). The hanging wall portion of the fracture trace map has been divided into four domains (I, II, III, and IV) based on the change in bedding strike across the map area.

Hanging Wall Structures. Two primary fracture sets occur in the hanging wall of the SBPF at the fracture trace map location (fig. 7). These include a set striking nearly parallel to the strike of the SBPF (Set A) and a set at a high angle to the SBPF (Set B). A discussion of the fracture properties of both sets of fracture follows and is summarized in table 1.

Both fracture sets have steep dips, generally greater than 80°. Set A maintains a constant strike sub-parallel to the strike of the SBPF. The strike of Set B, however, changes across the fracture trace map area. The fracture map and corresponding equal-area stereonet projections (fig. 7) show a change in orientation of Set B from north-northwest in domains I and II to north-northeast in domains III and IV. This change to a more northeast strike of Set B, when approaching the SBPF from the south, mimics the change in strike of the bedding units previously discussed.

Individual fractures within Set A generally have a very linear surface trace, whereas Set B fractures have a more undulatory surface trace. Within the fine-grained sandstone, the trace length of Set A ranges from inches to several feet. The trace length of individual fractures within Set B ranges from inches to tens of feet.

Spacing of Set A fractures is relatively consistent across most of the fracture trace map area and is approximately 8 to 12 inches. In domain I, the spacing of Set A fractures appears somewhat smaller on the order of 4 to 6 inches. The spacing of Set B is highly variable across the area, but in general is on the order of 12 to 24 inches. A green-gray, clayey infilling was observed in many fractures in the detailed study area. Field observations indicate this green-gray infilling occurs more often in Set B. Fracture surfaces of both sets commonly have a white-to-pale green surface coating or bleaching.

Fractures in the trace map area do not possess abundant surface markings or other features to aid in evaluating the mode of fracturing (i.e., modes I, II, or III; see Pollard and Aydin, 1988). Pinnate or feather structures (e.g., Hancock, 1985) indicating a shear component, were observed on several Set A fractures indicating a shearing mode. Surface markings such as plumose structures (e.g., arrest lines, hackle marks) indicative of an opening mode were rarely observed on fractures in the trace map area. A systematic and detailed analysis of individual fracture surfaces will be necessary to fully evaluate the mode(s) of fracture formation.

Fracture crosscutting and fracture termination relationships in the hanging wall suggest Set A fractures, which parallel the SBPF, are generally younger than Set B fractures. This conclusion is based on several observations: 1) Set A terminates against Set B in many cases; 2) Set A fractures locally offset Set B fractures; and, 3) the strike of Set B fractures changes orientation near the SBPF similar to the stratigraphic units defining the outcrop-scale syncline at location 4. In contrast, the strike of Set A fractures maintains a constant orientation across the fracture trace map area. These facts indicate Set B fractures were deformed during folding of the outcrop-scale syncline, whereas Set A fractures were unaffected by this folding (fig. 7).

Table 1. Summary table of fracture properties for fracture Sets A and B in the fracture trace map area in the hanging wall of the the SBPF shown in figure 7 (location 4, plate 2).

	<u>FRACTURE SET A</u>	<u>FRACTURE SET B</u>
Strike	WNW. - uniform	NNW.-NE. - variable
Dip	>80° - mainly S.	>80° - variable
Surface Trace	linear	undulatory
Trace Length	<0.5 ft to ~ 6.0 feet	<0.5 ft to ~10.0 feet
Spacing	4 to 12 inches	12 to 24 inches
Infilling	clayey, green-gray	clayey, green-gray (more common)
Wall Bleaching	white to green	white to green
Structures	pinnate and feather	not observed
Terminations	mainly A against B	few B against A
Offsets	A offsets B	----
Mode	opening and shearing	opening and shearing (?)
Relative Age	A mainly younger than B	some B coeval with A

Footwall Structures. Detailed mapping in the footwall portion of the fracture trace map area was limited to an 8 foot by 8 foot area immediately north of the SBPF at location 4 (plate 2) in a medium- to coarse-grained sandstone. The footwall structures contrast with those in the hanging wall portion of the map (figs. 7 and 12). For example, the pervasive, rectilinear hanging wall fracture Sets A and B were not observed in this portion of the footwall. Footwall structures and their orientations are shown in a 1:15-scale map (fig. 12) and the attributes of several of these features are briefly discussed below.

Fractures a, b, and c have a general northeast strike and are vertical. They have undulating surfaces, with a relatively wide, green-gray clayey infilling (up to green-gray clay. These fractures bound blocks of sandstone containing unfilled fractures of various orientations. Fractures d-i strike nearly east and are vertical. These fractures have relatively planar surfaces with 0.5 inch-wide, green-gray clayey infilling. These fractures terminate abruptly against fracture c and the feature Σ.

Fractures j and k strike nearly parallel (N. 70° W.) to the SBPF with a steep dip. Fracture j has a variable aperture which is partly filled with a green-gray, clayey material. Associated with j are minor fractures oriented N. 40°-50° W. Also associated with j are asymmetric, clayey bodies. Fracture k is nearly vertical with a

variable aperture with a green-gray, clayey infilling. The orientation of fracture k changes from a strike nearly parallel to the SBPF to a northeast strike near feature Ψ . Feature Ψ on the map is an asymmetric-shaped block of sandstone bounded by fractures.

Feature Σ is a folded green-gray, clayey layer. The fold has a 90° plunge with an axial plane oriented N. 45° E. 90° . The fold is asymmetric with a sense of vergence towards the east-southeast.

Structure Ω includes five curving fractures (labeled 1-5 on figure 12) that terminate against the SBPF. The angle between these fractures and the SBPF decreases from northwest to southeast, with fracture 1 having the largest angular difference of 64° and fracture 5 having the smallest angular difference of 28° .

DISCUSSION

Geologic mapping and structural analyses at locations 2, 4, 6, and 7 (plate 2) suggest at least two stages of faulting with associated folding and fracturing are represented by structures in the study area. Fault A, the northeast-striking fault terminating against the SBPF at location 4 (plate 2), represents normal faulting during stage 1. Stage 1 faulting is interpreted to be associated with longitudinal faulting and tilting of beds within the Deep River Triassic basin. Stage 2 represents a later phase of transverse faulting along the SBPF involving both normal and dextral strike-slip components of displacement that produced map-scale anticlinal folding and outcrop-scale synclinal folding in the hanging wall of the SBPF.

Table 2 shows the interpreted genetic relationships between structures, dominant fracture sets, and tectonic processes for features in the study area whose relative ages could be constrained by field data. Figure 13 shows a simplified schematic diagram for the proposed kinematic model. Faults B and C are not included in this model because their relationships to fault A and the SBPF could not be determined from the available data.

Table 2. Table relating structures, primary fracture sets, and tectonic processes for features in the study area whose relative ages could be interpreted from field relationships.

	<u>STRUCTURES</u>	<u>PRIMARY FRACTURE SETS</u>	<u>TECTONIC PROCESSES</u>
Stage 1	Fault A: NE.-striking normal faulting	N. to NE.-striking opening mode fractures	basin opening, longitudinal faulting, bed tilting
Stage 2A	SBPF: WNW.-striking normal faulting, hanging wall anticline	E.-striking opening mode fractures	transverse faulting, map-scale folding
Stage 2B	SBPF: WNW.-striking dextral strike-slip faulting, hanging wall syncline	E. and N.-striking shearing mode fractures	transverse faulting, outcrop-scale folding, reactivation of fault A

STAGE 1

We interpret the early movement along fault A to be normal displacement, longitudinal to the Deep River Triassic basin and antithetic to the Jonesboro fault (figs. 2 and 13). Although kinematic indicators for fault A are limited, features interpreted as drag folds (cross sections X-X' and Y-Y') indicate normal movement (down to the east).

Early movement along fault A predates displacement along the SBPF, which cross-cuts fault A (fig. 6). The majority of north-striking fractures throughout the study area are attributed to stage 1 processes related to extensional, longitudinal faulting and the eastward tilting of beds that predates transverse faulting along the SBPF. At location 4 (plate 2), north-striking fractures (Set B, fig. 7) generally predate east-striking fractures (Set A, fig. 8) associated with the SBPF. The general change in the orientation of north-striking fractures to a more northwest strike along a south-to-north traverse across the south borrow pit mimics the change in the orientation of the beds forming the anticline in the hanging wall of the SBPF (plate 2). This parallel change in the orientation of bedding and fractures further supports the interpretation that a north-striking fracture set predates the SBPF.

STAGE 2

Stage 2 corresponds to movement along the SBPF transverse to the strike of the Deep River Triassic basin. Our structural analysis suggests displacement along the SBPF involved both normal, and dextral strike-slip components (fig. 13). Normal displacement along the SBPF resulted in the map-scale anticline in the hanging wall of the SBPF (plate 2), and the corresponding east-striking, opening mode fractures. Dextral strike-slip movement along the SBPF resulted in the outcrop-scale synclines at locations 1 and 4 on plate 2 (figs. 4, 6, and 7), and the corresponding east-striking, shearing mode fractures. The relative timing of the normal and strike-slip movement along the SBPF could not be determined conclusively from the available data. The 70° rake measured on southwest plunging slickenlines on a fault plane oriented N. 85° W. 57° S. (location 7, plate 2) indicates a phase of synchronous dip-slip and dextral strike-slip displacement on the SBPF.

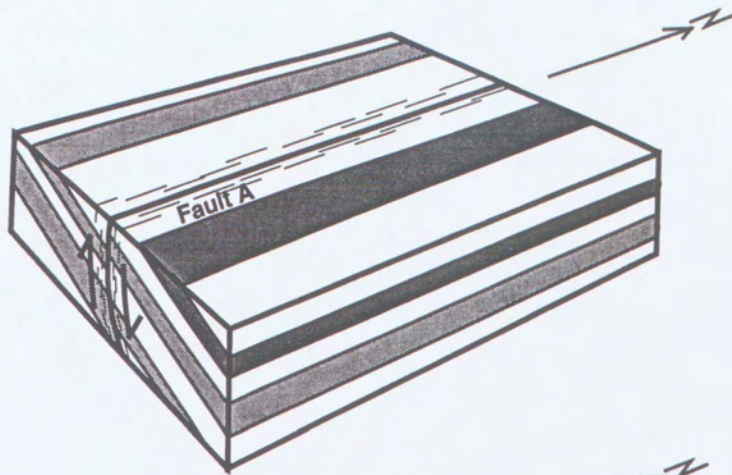
Stage 2 Normal Faulting

The interpretation that the map-scale anticlinal folding is related to normal faulting is consistent with the style of extensional basins such as the Deep River Triassic basin. Concentration of deformation in the hanging wall is commonly observed along normal faults, and particularly in cases where rollover structures are formed (e.g., Davis, 1984; Hatcher, 1995).

Fractures in the hanging wall portion of the fracture trace map area (fig. 7)

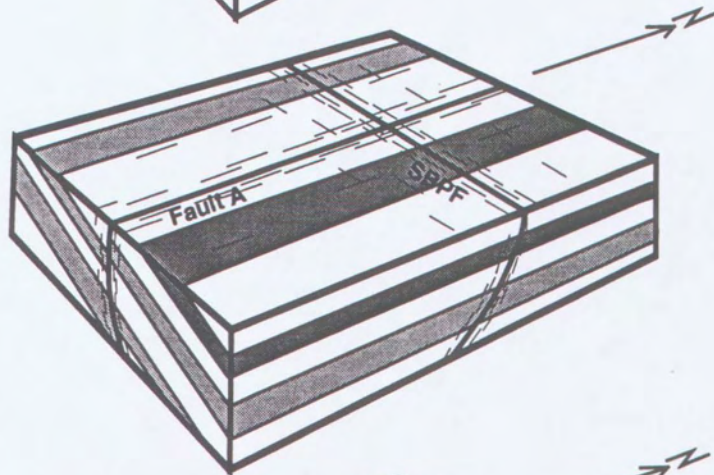
Stage 1:

- Longitudinal basin faulting (Fault A)
- Tilting of beds
- Formation of north-striking, opening-mode fractures.



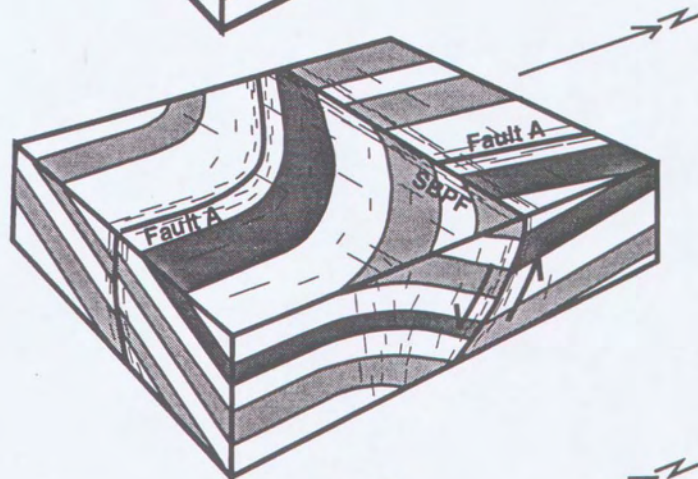
Stage 2:

- Transverse basin faulting
- Initial formation of south borrow pit fault (SBPF).
- East-striking, opening mode fractures



Stage 2A:

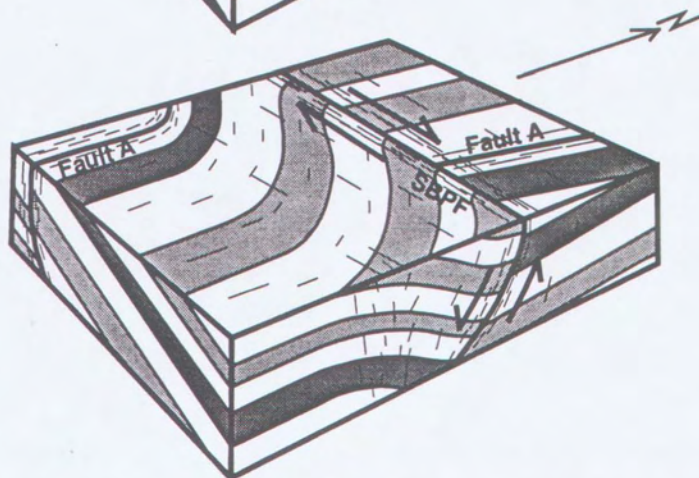
- Normal faulting
- Formation of map-scale, hanging wall anticline.
- East-striking, opening mode fractures.



Stages 2A and 2B may be coeval.

Stage 2B:

- Continued movement along SBPF.
- Dextral, strike-slip faulting;
- Formation of outcrop-scale, hanging wall syncline.
- East- and north-striking shearing mode fractures.



Stages 2A and 2B may be coeval.

Figure 13. Schematic diagram showing a possible kinematic model for the south borrow pit fault and associated structures.

also provide information about displacement along the SBPF. Field observations indicate the east-striking Set A fractures occur more commonly in the hanging wall than the footwall of the SBPF. This fact, and their orientation parallel to the SBPF, is consistent with their origin as opening mode fractures in the hanging wall of a normal fault. The concept of normal displacement along the SBPF is further supported by east-striking Set A fractures that offset north-striking Set B fractures with a normal sense of displacement observed at location 4 (plate 2).

The map pattern produced by the hanging wall anticline could also have been produced by drag folding related to reverse faulting, or sinistral strike-slip faulting along the SBPF. Aside from the geometry of the map-scale fold, no evidence for reverse faulting or sinistral strike-slip faulting was observed along the SBPF. Previous studies in the Deep River Triassic basin (e.g., Reinemund, 1955) have not documented significant reverse or thrust faulting. Thrust faults were observed in trenches at the proposed Wake/Chatham LLRW site, but are generally interpreted to be very minor in significance (Chem-Nuclear Systems, Inc., 1993). A component of sinistral strike-slip displacement was reported by Ebasco Services, Inc. (1975) along the Harris fault and Chem-Nuclear Systems, Inc. (1993) presented evidence for sinistral strike-slip displacement on the W82 fault.

Stage 2 Strike-slip Faulting

Kinematic indicators at locations 2, 4, and 7 (plate 1) as well as the "right-stepping" outcrop pattern (see McClay, 1987) of the SBPF, indicate evidence for a component of dextral strike-slip or dextral-normal oblique faulting along the SBPF. Evidence for dextral strike-slip faulting occurs in both the hanging wall and footwall of the SBPF.

The geometry of the outcrop-scale syncline in the hanging wall of the SBPF at location 4 (plate 2) shown in figures 6 and 7 suggests it formed by drag related to dextral strike-slip faulting. This fold geometry, however, could also be explained by drag during normal faulting. The orientation of the fold hinge (N. 83° E. 9°) for this structure, however, appears to more consistent with the shortening direction expected in a dextral strike-slip system. The orientation of pinnate structures on several east-striking, Set A fractures are consistent with fracture formation during dextral strike-slip faulting. In addition, some north-striking, Set B fractures are offset in a dextral sense by Set A fractures. The change in orientation of north-striking fractures in the outcrop-scale syncline (Set B, fig. 7) is also consistent with the concept of dextral strike-slip displacement.

The asymmetry of sigmoidal-shaped sandstone bodies observed at location 2 (fig. 5) and locations 4 and 7 also suggest dextral strike-slip faulting. In addition, the geometry of fractures at location 2 are consistent with orientation of fractures expected in a dextral, Riedel shear system (inset, fig. 5). The sigmoidal shape and asymmetry of the sandstone body at location 2, however, can also be explained by a sandstone body bounded by two closely spaced, normal faults.

Termination relationships between east-striking, Set A fractures and north-striking, Set B fractures observed in outcrop at location 6 (plate 2) and summarized in figure 10 indicate that at some locations the two fracture sets may have developed simultaneously during movement along the SBPF. Similarly, at location 4 (plate 2) a limited number of Set B fractures terminate against Set A fractures. Given these indications of overlapping development, some north-striking fractures may be localized shearing mode fractures developed during strike-slip movement along the SBPF (i.e., R_2 Riedel fractures).

Structural features observed in the footwall of the SBPF also suggest dextral strike-slip displacement along the SBPF (fig. 12). Fractures at location j, and structures Ψ , Ω , Σ are particularly illustrative. The fractures at location j in figure 12 are interpreted as pinnate fractures or conjugate shear fractures and their geometry and sense of displacement are consistent with dextral shearing. Likewise, the asymmetry (S-shape) of the sigmoidal clay-filled fractures associated with structure Ψ also suggest dextral shearing. Structure Ψ is interpreted as a fault bounded block (e.g., horse block). The S-shape asymmetry of this block also supports dextral strike-slip shearing.

Structure Ω is interpreted as a contractional strike-slip duplex similar to those described by Woodcock and Fischer (1986) and also indicates a dextral sense of displacement. The duplex comprises fractures (1-5 on fig. 12), interpreted as faults, that sole into the SBPF. The angle between each fault and the SBPF increases from fault 5 to fault 1. This change in angle is interpreted to reflect the steepening of earlier faults (e.g., 1) because of emplacement of later faults (2-5) during a forward-breaking sequence similar to that observed in foreland thrust systems.

The formation and geometry of the folded clayey layer (Σ on figure 12) is likely to be related to the duplex structure Ω , similar to fault related folds developed in foreland thrust systems. The geometry of the folded clayey layer Σ , including its vertically plunging fold hinge, the axial surface orientation (N. 45° E. 90°), and the sense of asymmetry or vergence suggests dextral strike-slip displacement.

KINEMATIC MODEL

Based on available data and the interpretations presented above we suggest a kinematic model for the study area that includes normal faulting (fault A) during stage 1, and a combination of normal and dextral strike-slip faulting (SBPF) during stage 2. It is likely stage 2 displacement occurred during a single deformation event with components of normal, dextral, and dextral-normal oblique displacement occurring at different locations and relative times along the SBPF during this event (fig. 13). The sense of drag observed in the map- and outcrop-scale folds along the SBPF is a function of the geometry between the attitude of the stratigraphic marker units and the SBPF. This requires that stratigraphic markers were either tilted eastward prior to displacement or the entire area was tilted after faulting had

occurred. In our model, the eastward tilting of the beds is associated with stage 1 longitudinal faulting.

The total displacements along the SBPF and other faults reported here are not determinable from the available data. We interpret the relative magnitude of normal displacement along the SBPF to be greater than the magnitude of strike-slip displacement given the hanging wall anticline (inferred to be the result of normal displacement) is a map-scale feature in contrast to the smaller, outcrop-scale synclines related to strike-slip movement.

This basic kinematic model accounts for the map patterns and structural features observed at the surface in the south borrow pit. A northwest-striking normal fault (fault B) and a northeast-striking reverse(?), sinistral strike-slip fault (fault C) were identified in the study area. Further work will be required to determine any relationships of these structures to fault A and the SBPF.

SUMMARY

Geologic mapping of Triassic-age rocks at two very well exposed areas in the New Hill and Cokesbury 7.5-minute quadrangles identified stratigraphic marker units, map and outcrop-scale folding, and four previously unreported faults. The results of this investigation are summarized as follows:

- Mappable stratigraphic marker units within a heterogeneous, siliciclastic sequence include conglomeratic sandstone, (muddy) sandstone, siltstone, and mudstone. Some stratigraphic units, even some less than six feet thick, can be traced along strike for several hundreds of feet in the map area.
- Three faults were identified in the south borrow pit (SBPF, faults A and B) and one fault (fault C) was identified in the north borrow pit. The south borrow pit fault (SBPF) strikes nearly east-west, dips south, and has a minimum trace length of 1,400 feet across the south borrow pit. Faults A, B, and C are high-angle faults that strike oblique to the SBPF. Fault A terminates against the SBPF. Further studies are needed to identify the extent and other possible structural components of these faults, and to resolve their tectonic relationships.
- A map-scale fold in the hanging wall of the SBPF is interpreted as a hanging wall anticline developed during normal displacement along the SBPF. This map-scale folding resulted in northwest-striking beds that differ from the overall north- to northeast-striking map units defined by previous work in the area. The outcrop-scale folds in the hanging wall of the SBPF are interpreted as synclinal folds developed during dextral strike-slip movement along the SBPF.

- Numerous kinematic indicators suggest components of normal and dextral strike-slip movement along the SBPF. The relative magnitude of normal displacement along the SBPF is interpreted to be greater than the magnitude of strike-slip displacement. The total displacements along the SBPF and other faults reported here are not determinable from the available data.
- Limited data and analyses indicate both normal and dextral strike-slip components of displacement along fault A. The dextral strike-slip component of displacement may be associated with reactivation of fault A during movement along the SBPF. Movement along fault B is interpreted as normal. Displacement along fault C is interpreted to have both reverse and sinistral components.
- Two dominant fracture sets are observed in the study area. One east-striking set is sub-parallel to, and genetically related to the SBPF. The other set strikes generally north, oblique to the SBPF, and is interpreted to have formed primarily prior to movement along the SBPF. Some of the fractures oblique to the SBPF appear to have formed at the same time as those fractures sub-parallel to the SBPF.
- In general, the spacing of fractures parallel to the the SBPF decreases with proximity to the fault. Adjacent to the SBPF the spacing is on the order of 4 to 12 inches.
- Kinematic studies suggest at least two stages of faulting with associated folding and fracturing are represented by structures in the study area. Stage 1 faulting (e.g., fault A) is interpreted to be associated with longitudinal normal faulting and tilting of beds within the Deep River Triassic basin. Stage 2 represents a later phase of transverse faulting along the SBPF involving both normal and dextral strike-slip components of displacement.
- The four newly discovered faults from this study, along with other faults previously identified in the area, indicate this portion of the Deep River Triassic basin is in structurally complex zone of intersecting faults.

ACKNOWLEDGEMENTS

This report benefited greatly from reviews by Charles Gardner, Jeff Reid, Albert Carpenter, Kathleen Farrell, Bill Hoffman, Mike Medina, and Leonard Wiener. Discussions in the field with Kathleen Farrell, Jim Hibbard, and Peter Malin resulted in major improvements to the report. Access to the study area provided by Carolina Power and Light and Chem-Nuclear Systems, Inc. is gratefully acknowledged. Law Engineering provided the color negative used to produce the 1:6,000 scale color aerial photograph enlargement of the study area.

REFERENCES CITED

- Allmendinger, R. W., 1995, Stereonet Ver. 4.9 - a plotting program for orientation data for the Macintosh™ computers, stereonet 4.5 disk manual: Cornell University, Ithaca, New York, 44 p.
- American Society for Testing and Materials, 1989, Standard practice for description and identification of soils (visual-manual procedure) Designation D 2488 - 84e1, *in* Annual Book of ASTM Standards, v. 4.08, Soil and Rock; Building Stones; Geotextiles, 997 p.
- Arbogast, J.S., 1976, Fluvial deposition of Triassic red beds, Durham basin, North Carolina: Durham, Duke University, M.S. thesis, 117 p.
- Bain, G.L., and Brown, C.E., 1980, Evaluation of the Durham Triassic Basin of North Carolina and techniques to characterize its waste-storage potential: U.S. Geological Survey, Open-File Report 80-1295, 133 p.
- Bain, G.L. and Harvey, B.W., eds., 1977, Field guide to the geology of the Durham Triassic basin: Carolina Geological Society, Fortieth Annual Meeting, 7-9 October 1977, North Carolina Department of Natural Resources and Community Development, Division of Earth Resources, Geology and Mineral Resources, 83 p.
- Barton, C.C., Larsen, E., Page, W.R., and Howard, T.M., 1993, Characterizing fractured rock for fluid-flow, geochemical, and paleostress modeling: Methods and preliminary results from Yucca Mountain, Nevada: U.S. Geological Survey Open-File Report 93-269, 62 p.
- Campbell, M.R., and Kimball, K.W., 1923, The Deep River coal field of North Carolina: North Carolina Geological and Economic Survey, Bulletin 33, 95 p.
- Chem-Nuclear Systems, Inc., 1993, License application North Carolina low-level radioactive waste disposal facility Wake/Chatham County preferred site, Revision 1, submitted to Division of Radiation Protection, North Carolina Department of Environment, Health and Natural Resources: Raleigh, North Carolina, Chem-Nuclear Systems, Incorporated.
- Compton, R.R., 1962, Manual of field geology: New York, John Wiley and Sons, 378 p.
- Davis, G.H., 1984, Structural geology of rocks and regions: New York, John Wiley & Sons, 492 p.
- Ebasco Services, Inc., 1975, Fault investigation - Shearon Harris Nuclear Power Plant, New Hill: Ebasco Services, Inc., 620 p.

- Folk, R.L., 1974, Petrology of sedimentary rocks: Hemphill Publishing Co., 182 p.
- Folk, R.L., 1980, Petrology of sedimentary rocks: Hemphill Publishing Co., 182 p.
- Gore, P.J.W., 1986, Depositional framework of a Triassic rift basin: The Durham and Sanford sub-basins of the Deep River basin, North Carolina, *in* Textoris, D. A., ed., Society of Economic Paleontologists and Mineralogists Field Guidebook, Third Annual Midyear Meeting, Raleigh, North Carolina, p. 53-115.
- Hancock, P.L., 1985, Brittle microtectonics: Principles and practice: *Journal of Structural Geology*, v. 7, p. 437-457.
- Hatcher, R.D., Jr., 1995, Structural geology: Principles, concepts, and problems: Englewood Cliffs, Prentice Hall, 525 p.
- Hoffman, C.W., and Gallagher, P.E., 1989, Geology of the Southeast Durham and Southwest Durham 7.5-minute quadrangles, North Carolina: *North Carolina Geological Survey Bulletin* 92, 34 p.
- Hu, L.N., and Textoris, D.A., 1994, Cycles in lake beds of the Triassic Sanford sub-basin of North Carolina, *in* Dennison, J.M., and Ettensohn, F.R., Controls on sedimentary cycles: *SEPM Concepts in Sedimentology and Paleontology*, v.4, p. 5-23.
- Huber, P., Lucas, S.G., and Hunt, A.P., 1993, Revised age correlation of the Upper Triassic Chatham Group (Deep River Basin, Newark Supergroup), North Carolina: *Southeastern Geology*, v. 33, no. 4, p. 171-193.
- La Pointe, P.R., and Hudson, J.A., 1985, Characterization and interpretation of rock mass joint patterns: *Geological Society of America Special Paper* 199, 37 p.
- Luttrell, G.W., 1989, Stratigraphic nomenclature of the Newark Supergroup of eastern North America: *U.S. Geological Survey Bulletin* 1572, 136 p.
- McClay, K.R., 1987, The mapping of geological structures: Halsted Press, New York, 161 p.
- North Carolina Geological Survey, 1985, Geologic Map of North Carolina: Department of Natural Resources and Community Development, Raleigh, North Carolina, scale 1:500,000.
- Olsen, P.E., 1978, On the use of the term Newark for Triassic and Early Jurassic rocks in eastern North America: *Newsletters on Stratigraphy*, v. 7, no. 2, p. 90-95.

- Olsen, P.E., Froelich, A.J., Daniels, D.L., Smoot, J.P., and Gore, P.J.W., 1991, Rift basins of early Mesozoic age, *in* Horton, J.W., and Zullo, V.A., eds., *The Geology of the Carolinas*: University of Tennessee Press, Knoxville, Tennessee, p. 142-170.
- Parker, J.M., III, 1979, *Geology and mineral resources of Wake County*: North Carolina Geological Survey Bulletin 86, 122 p.
- Pollard, D.D., and Aydin, A., 1988, Progress in understanding jointing over the past century: *Geological Society of America Bulletin*, v. 100, p. 1181-1204.
- Reinemund, J.A., 1955, *Geology of the Deep River Coal Field, North Carolina*: U. S. Geological Survey Professional Paper 246, 159 p.
- Schlische, R.W., 1995, Geometry and origin of fault-related folds in extensional settings: *American Association of Petroleum Geologists Bulletin*, v. 79 p. 1661-1668.
- Sibson, R.H., 1977, Fault rocks and fault mechanisms: *Journal of the Geological Society of London*, v. 133, p. 191-214.
- Textoris, D.A., and Gore, P.J.W., 1994, Upper Triassic organic-rich lake, Sanford sub-basin, North Carolina, U.S.A, *in* *Global geological record of lake basins*: Cambridge, Cambridge University Press, p. 173-177.
- Textoris, D.A., and Robbins, E.I., 1988, Coal resources of the Triassic Deep River basin, North Carolina: U.S. Geological Survey Open-File Report 88-682, 16 p.
- Wheeler, W.H., and Textoris, D.A., 1978, Triassic limestone and chert of playa origin in North Carolina: *Journal of Sedimentary Petrology*, v. 48, p. 765-776.
- Williamson, D.A., 1984, Unified rock classification system: *Bulletin of the Association of Engineering Geologists*, vol. XXI, p 253-254.
- Woodcock, N.H., and Fischer, M., 1986, Strike-slip duplexes: *Journal of Structural Geology*, v. 8, p. 725-735.

APPENDICES

APPENDIX A: STRUCTURE DATA - NORTH BORROW PIT (see figure 11)

STATION NUMBER	ROCK TYPE*	BEDDING ATTITUDE	FRACTURE ATTITUDE	FRACTURE ATTITUDE	FRACTURE ATTITUDE	FAULT ATTITUDE	AXIAL PLANE OF FOLD	FOLD AXIS TREND & PLUNGE
NB1	ss		010/90	080/90				
NB2	css/ss	310/20n	010/90	090/90	335/90			
NB3	ss/ms		340/70 s	080/90				
NB4			352/73 n	075/85 s				
			350/56 s	079/87 s				
NB5	ss/mss		314/77 n					
		350/05 n	282/90	060/90	016/90			
		005/10 s	348/90	075/90	005/86 s			
NB6	css		354/80 e	027/57 n				
	ss	030/12 s	350/90	033/90	077/90			
NB7	ms		350/90					
NB8			340/90	75/90				
NB9	ss	316/10 n	000/90	350/90				
NB10	css		070/90	345/90				
NB11	css		085/90	023/90				
NB12	css	010/16 s	082/90					
NB13	ms/ss	340/20 n	088/90	282/90	346/90			
NB14			025/90					
NB15	css/ms	047/25 s	340/85 n	080/72 n				
	css/mss	335/08 n	315/90	072/90	342/90			
NB16	ms		340/90					
NB17	ss		000/90					
NB18	mss		350/90	086/90				
NB19	mss		000/90					
NB20			075/90					
NB21	ms		335/90					
NB22	sms		003/90					
NB23		015/20 s	070/85 s	332/75 n	343/15 n			
			078/80 s	346/89 n	337/04 n			
			082/81 n	356/85 n				
			180/84 n	332/75 n				
			078/80 s					
NB24		330/22 n	348/80 s	180/90	030/75 s			
			345/90	080/90				
			345/72 s					
		282/09 s	335/74 s	077/90	045/90	005/90		
			326/60 s					
			330/75 s					
	ss		070/90					
	ss		080/90					
	css		000/80 s					
	css	070/10 s						

*Rock Type: css-conglomeratic sandstone, ss-sandstone, mss-muddy sandstone, sl-siltstone, ms-mudstone

APPENDIX A: STRUCTURE DATA - NORTH BORROW PIT (see figure 11)

STATION NUMBER	ROCK TYPE*	BEDDING ATTITUDE	FRACTURE ATTITUDE	FRACTURE ATTITUDE	FRACTURE ATTITUDE	FRACTURE ATTITUDE	FRACTURE ATTITUDE	FRACTURE ATTITUDE	FAULT ATTITUDE	AXIAL PLANE OF FOLD	FOLD AXIS TREND & PLUNGE
NB25		300/12 n	013/85 s	059/85 n	303/90						
		338/15 n	022/85 s	066/89 n	340/81 s						
				078/88 s	327/72 s						
				075/90	335/85 s						
NB26	mss	295/15 n	324/90	082/90	342/90						
		020/15 s		317/90							
		339/08 n									
		334/20 n	080/87 s	345/70 s	071/90	332/90					
NB27	ss	307/25 n	086/85 s	336/69 s							
		332/30 n									
		020/08 s	338/85 n	068/85 n							
		017/10 s	340/78 n	078/90							
NB28	mss	288/26 n									
			005/75 s	343/90	065/90	058/90					
			060/90	022/90	330/90						
			005/90	275/90							
NB29	mss/ss		355/90	300/90							
			350/90	020/90							
			345/90	075/90							
			340/90	070/90	045/80 n						
NB30	ss		076/78 s	027/90	323/76 s	298/90					
			002/70 n	080/90	353/85 s						
			012/78 n								
			075/90	305/90	340/90						
NB31	ss	084/32 n									
		051/39 n									
		070/33 s									
		068/50 n									
NB32	mss	320/35 n									
		066/34 s									
		276/80 n									
		064/36 s									
NB33	mss	300/55 n	285/90								
			015/90								
			359/51 w	082/90	329/60 n	072/05 s					
			355/60 n	084/64 s	322/60 n						
NB34	mss	349/60 n									
		352/52 n									
NB35	mss	342/15 n									
NB36	ss										
NB37	mss										
NB38	mss										
NB39	mss										

*Rock Type: css-conglomeratic sandstone, ss-sandstone, mss-muddy sandstone, sl-siltstone, ms-mudstone

APPENDIX A: STRUCTURE DATA - NORTH BORROW PIT (see figure 11)

STATION NUMBER	ROCK TYPE*	BEDDING ATTITUDE	FRACTURE ATTITUDE	FRACTURE ATTITUDE	FRACTURE ATTITUDE	FRACTURE ATTITUDE	FAULT ATTITUDE	AXIAL PLANE OF FOLD	FOLD AXIS TREND & PLUNGE
NB40	ms ss/ms	010/13s 065/56n 060/10n	030/80 e	350/55 e					
NB41	ss/ms	345/16n	358/80 w						
NB42	ss/ms	010/12n 050/20n							
NB43	ss		310/75 s						
NB44	mss	000/10e							
NB45	ss/mss	345/08n	335/80 s						
NB46	css		350/80 s	080/90					
NB47		084/32 n							

*Rock Type: css-conglomeratic sandstone, ss-sandstone, mss-muddy sandstone, sl-siltstone, ms-mudstone

APPENDIX A: STRUCTURE DATA - SOUTH BORROW PIT (see figure 11)

STATION NUMBER	ROCK TYPE*	BEDDING ATTITUDE	FRACTURE ATTITUDE	FRACTURE ATTITUDE	FRACTURE ATTITUDE	FRACTURE ATTITUDE	FAULT ATTITUDE	RAKE OF SLICKENLINES
SB1	ss/ss	310/28 n						
	mss		042/90					
SB2	mss		310/90					
	ss		290/90					
	ss		025/90					
		305/20 n						
	ss		016/45 s					
	ss		313/75 n					
		017/24 s						
	css/ms	300/18 n		346/69 n				
	sms	310/14 n		351/72 s				
				278/90				
SB3			312/90					
	sl		315/90				80/55 s	
	sl		305/90		293/90			
	ss	330/18 e		285/90		070/90		
				350/90				
				085/65 s				
	mss/ss	018/28 s		295/70 s		043/60 w		
	css							
	ms/ss	358/29 e						
	ss	042/40 s						
	ss	000/12 e		085/65 s				
	ss	027/18 s		180/80 w				
SB4	ss							
	sl	330/18 n		350/90				
	ss			315/55 s		295/90		060/42 s
SB5	ss			305/65 s		008/90		030/030 s
	ss							
SB6		013/13 s						
		354/25 n						
SB7	sl	296/30 n						
	sl	013/19 s						
	ms	013/13 s						
		012/14 s						
	ss	282/10 n		295/90		040/90		290/55 s

*Rock Type: css-conglomeratic sandstone, ss-sandstone, mss-muddy sandstone, sl-siltstone, ms-mudstone

APPENDIX A: STRUCTURE DATA - SOUTH BORROW PIT (see figure 11)

STATION NUMBER	ROCK TYPE*	BEDDING ATTITUDE	FRACTURE ATTITUDE	FRACTURE ATTITUDE	FRACTURE ATTITUDE	FRACTURE ATTITUDE	FAULT ATTITUDE	RAKE OF SLICKENLINES
SB8	sl	020/25 s						
	ss	340/70 s						
	ss	290/54 s						
	ms	036/52 s						
	ss	001/10 s						
	ms	000/45 w						
			340/80 n					
			020/36 s					
	ss/ms	020/20 s	295/90	025/90				
	ss	008/10 s	305/60 s				290 55 s	
SB9		020/25 s						
	ss	345/22 n	275/75 s					
			010/90					
			026/90					
SB10	sts/lss	353/07 n	320/65 s					
		345/54 n						
		014/56 s						
		010/80 s						
		345 70 n						
		020/70 s						
		290/54 s						
		020/20 s						
		020/25 s						
		035/52 s						
		275/15 s						
		020/15 s						
SB11		020/36 s						
		345/80 n						
		000/90						
		005/54 n						
		010/50 s						
SB12	see Appendix B	345/67 n	040/90	080/90	340/90			
	mss/ms							

*Rock Type: css-conglomeratic sandstone, ss-sandstone, mss-muddy sandstone, sl-siltstone, ms-mudstone

APPENDIX A: STRUCTURE DATA - SOUTH BORROW PIT (see figure 11)

STATION NUMBER	ROCK TYPE*	BEDDING ATTITUDE	FRACTURE ATTITUDE	FRACTURE ATTITUDE	FRACTURE ATTITUDE	FRACTURE ATTITUDE	FAULT ATTITUDE	RAKE OF SLICKENLINES
SB14	ss		012/90 270/90					
SB15	ss	010/18 s 010/15 s		280/90 335/90				
SB16			008/78 n		033/90			
SB17			325/90 330/90					
SB18	sms/ms	340/15 n	034/90 305/90					
SB19	ms	342/15 n	008/78 n					
SB20	ms	342/15 n	353/90					
SB21	mss	300/40 s	325/90				335/85 s	
SB22	sl ss/sl	276/85 s 050/65 n 295/30 n	276/70 s				080/85 s	
SB23		013/19 s 300/12 n						
SB24	ms	296/30 n		030/90				
SB25		010/25e	295/90 010/30 e					
SB26			050/90					
SB27	sms		317/90					
SB28	ms		012/90	276/90				
SB29	ms		020/90					
SB30			280/90					
SB31	sms/cs/ms	310/10 n	334/90	070/12				
	ss/ms	300/15 n	340/90	290/90				
	css	335/04 n						
	ss	326/20 n						
SB32	ms	353/19 e	350/90	035/90	007/90			
SB33	ms		350/90	35/90	353/90			
SB34			012/90	285/90	026/90			
SB35		307/20 n	022/90	051/90	332/85 s			
SB36		311/17 n	297/90	020/90				

*Rock Type: css-conglomeratic sandstone, ss-sandstone, mss-muddy sandstone, sl-siltstone, ms-mudstone

APPENDIX A: STRUCTURE DATA - SOUTH BORROW PIT (see figure 11)

STATION NUMBER	ROCK TYPE*	BEDDING ATTITUDE	FRACTURE ATTITUDE	FRACTURE ATTITUDE	FRACTURE ATTITUDE	FRACTURE ATTITUDE	FAULT ATTITUDE	RAKE OF SLICKENLINES
SB37	SS	020/10 s	312/90	281/90	320/90			
SB38	SS		004/78 n	320/11 s				
SB39	SS		310/90	010/90				
	SS	010/20 e						
	SS	358/12 w	310/90	040/90				
	SS	302/12 e						
	SS		008/90	082/90				
	SS		006/90	090/90				
	SS		010/90	050/90				
SB40			327/90					
SB41		007/35 s	325/90	080/90	344/68 s			
SB42		355/12 w	305/90	050/90				
SB43	ms		070/80 n	326/80w			330/29 s	150/29S/72
SB44	SS	000/20 e	010/70 s	275/90				
SB45	SS	005/13 e						
	SS	010/16 e						
SB46	SS		320/80 n	348/70s			275/57 s	275/57S/70
SB47	SS						090/70 s	270/70S/83
SB48	SS	005/30s	280/90	005/70s			290/58 s	
							278/65 s	
							082/63 s	
SB49	SS	330/10n						
SB50	SS	335/20n						
SB51	ss/ms	305/12n						
SB52	ss/ms	088/31s	275/90					
SB53	ms	345/12e						
SB54	ms	349/10e						
SB55	ms/ss	340/10e						
SB56	ss	315/5e						
SB57	ms/ss	345/15e	349/65 w	075/65n				
SB58	ms/ss	335/8e	345/90	065/90				
	ms/ss	000/14e	358/90	007/55w				
	SS		355/37 w					

*Rock Type: css-conglomeratic sandstone, ss-sandstone, mss-muddy sandstone, sl-siltstone, ms-mudstone

APPENDIX B: STRUCTURE DATA FOR FRACTURE TRACE MAP AT LOCATION 4 (see figure 7)

Domain I				Domain II			
Bedding attitudes	Fracture attitudes			Bedding attitudes	Fracture attitudes		
305 / 12 n	000 / 90	110 / 84 s	118 / 82 w	343 / 15 n	000 / 90	171 / 78 s	
306 / 15 n	001 / 90	110 / 84 s	119 / 82 w		000 / 90	172 / 68 s	
312 / 8 n	011 / 90	110 / 84 s	120 / 74 s		010 / 90	175 / 81 s	
319 / 9 n	012 / 90	111 / 72 s	121 / 66 s		010 / 90	176 / 82 s	
	014 / 90	111 / 72 s	144 / 60 s		012 / 90	178 / 82 s	
	014 / 90	111 / 80 s	181 / 79 n		012 / 90	184 / 69 n	
	014 / 90	112 / 68 s	181 / 85 n		012 / 90	184 / 74 n	
	015 / 90	112 / 76 s	184 / 58 n		019 / 90	185 / 81 n	
	018 / 90	112 / 84 s	191 / 68 n		021 / 90	189 / 76 n	
	019 / 90	112 / 84 w	191 / 70 n		021 / 90	192 / 80 n	
	021 / 90	112 / 85 s	192 / 82 n		022 / 90	199 / 68 n	
	021 / 90	114 / 70 s	194 / 80 n		102 / 83 s	280 / 90	
	021 / 90	114 / 74 s	196 / 81 n		106 / 85 s	281 / 90	
	021 / 90	114 / 74 s	279 / 90		108 / 76 s	286 / 90	
	024 / 90	114 / 75 s	282 / 90		109 / 76 s	289 / 90	
	029 / 90	114 / 76 s	286 / 90		109 / 85 s	294 / 90	
	029 / 90	114 / 76 s	290 / 90		109 / 85 s	295 / 90	
	029 / 90	114 / 76 s	292 / 90		110 / 83 s	295 / 90	
	030 / 64 s	114 / 76 s	292 / 90		111 / 76 s	341 / 90	
	076 / 90	114 / 77 s	293 / 90		111 / 80 s	345 / 90	
	076 / 90	114 / 77 s	295 / 72 n		111 / 81 s	351 / 90	
	076 / 90	114 / 78 s	296 / 90		111 / 81 s	351 / 90	
	096 / 84 s	115 / 70 s	299 / 90		111 / 87 s	354 / 90	
	099 / 85 s	115 / 71 s	305 / 90		112 / 71 s	354 / 90	
	103 / 76 s	115 / 72 s	342 / 90		112 / 72 s	356 / 90	
	104 / 72 s	115 / 75 s	344 / 90		112 / 75 s	358 / 90	
	104 / 74 s	115 / 80 s	346 / 90		112 / 82 s		
	105 / 75 s	115 / 80 s	354 / 90		112 / 82 s		
	105 / 76 s	116 / 71 s	355 / 90		112 / 84 s		
	105 / 80 s	116 / 71 s	356 / 65 n		112 / 85 s		
	105 / 83 s	116 / 77 s	356 / 72 n		112 / 85 s		
	105 / 85 s	116 / 77 s			113 / 80 s		
	106 / 71 s	116 / 78 s			114 / 81 s		
	106 / 74 s	116 / 80 s			114 / 82 s		
	106 / 74 s	116 / 80 s			114 / 84 s		
	106 / 74 s	116 / 80 w			114 / 85 s		
	106 / 81 s	116 / 80 w			115 / 74 s		
	106 / 85 s	116 / 81 s			115 / 76 s		
	109 / 74 s	116 / 84 s			115 / 88 s		
	109 / 79 s	117 / 82 s			116 / 76 s		
	109 / 81 s	118 / 70 w			116 / 76 s		
	110 / 72 s	118 / 76 w			116 / 81 s		
	110 / 76 s	118 / 77 s			118 / 79 s		
	110 / 76 s	118 / 80 w			169 / 71 s		
	110 / 78 s	118 / 80 w			169 / 84 s		

Domain III				Domain IV			
Bedding attitudes	Fracture attitudes			Bedding attitudes	Fracture attitudes		
005 / 10 s	000 / 90	115 / 80 s	196 / 86 n	018 / 12 s	025 / 90		
015 / 9 s	002 / 90	115 / 83 s	198 / 76 n	026 / 10 s	025 / 90		
	002 / 90	115 / 85 s	199 / 70 n		029 / 90		
	006 / 90	115 / 85 s	199 / 75 n		102 / 86 s		
	011 / 90	115 / 86 s	199 / 75 n		104 / 84 s		
	012 / 90	116 / 79 s	200 / 81 n		106 / 75 s		
	012 / 90	116 / 80 s	201 / 75 n		106 / 80 s		
	012 / 90	116 / 80 s	208 / 75 n		106 / 81 s		
	014 / 90	116 / 81 s	209 / 88 n		106 / 82 s		
	014 / 90	116 / 85 s	211 / 89 n		106 / 82 s		
	019 / 90	116 / 86 s	242 / 78 n		108 / 86 s		
	021 / 90	116 / 86 s	281 / 50 n		109 / 79 s		
	028 / 90	118 / 79 s	281 / 90		109 / 81 s		
	029 / 90	118 / 81 s	286 / 90		109 / 88 s		
	036 / 90	118 / 81 s	292 / 90		110 / 78 s		
	098 / 88 s	118 / 81 s	292 / 90		111 / 76 s		
	101 / 88 s	120 / 82 s	294 / 90		111 / 80 s		
	102 / 80 s	123 / 80 s	294 / 90		111 / 85 s		
	102 / 85 s	179 / 81 s	296 / 90		111 / 88 s		
	106 / 76 s	180 / 80 w	298 / 90		112 / 76 s		
	106 / 86 s	186 / 81 n	298 / 90		112 / 76 s		
	109 / 80 s	189 / 80 n	299 / 90		114 / 74 s		
	109 / 81 s	189 / 85 n	319 / 64 n		114 / 83 s		
	109 / 81 s	190 / 81 n	358 / 90		120 / 89 s		
	111 / 81 s	190 / 84 n			120 / 89 s		
	111 / 88 s	191 / 73 n			194 / 81 n		
	111 / 88 s	191 / 80 n			199 / 86 n		
	112 / 78 s	193 / 85 n			201 / 81 n		
	112 / 84 s	195 / 80 n			209 / 70 n		
	115 / 78 s	195 / 83 n			209 / 70 n		

APPENDIX C

WEATHERING AND ROCK MASS CLASSIFICATION

Excavation of the borrow pits in the mid- to late-1970's removed soil and weathered rock to estimated depths of 4 to 12 feet below the ground surface. Exposure of the previously weathered rock in the floor of the pits accelerated the normal weathering processes affecting the engineering properties of the rocks. The Unified Rock Classification System (URCS), developed by Williamson (1984), was applied at the reconnaissance level to describe the basic engineering properties of weathered rock units exposed in the borrow pits, and to supplement standard geologic classifications. The URCS rates four basic elements of the rock mass: 1) degree of weathering, 2) strength, 3) discontinuities, and 4) unit weight. A single letter abbreviation (A through E) is used for each of the four properties of the rock mass. Appendix C is a condensed version of the URCS adapted from Williamson (1984). In the following brief overview, the abbreviated rating for each category is shown in parentheses immediately after qualifiers in the text.

All rocks in the borrow pits show signs of weathering; however, weathering has not progressed sufficiently to develop a soil profile. In general, the degree of weathering of the rocks ranges from the stained state (C), through the partly decomposed state (D), to the completely decomposed state (E). Mineral components of stained state rocks are partly or completely discolored due to oxidation alteration. Partly decomposed rocks can be remolded into gravel or larger size pieces with finger pressure. Completely decomposed rocks can be remolded to sediment without gravel or larger size fragments with finger pressure. Resistant ledges or pavements of stained state rock are invariably conglomeratic sandstone or sandstone; however, these rocks types also occur in the partly decomposed and completely decomposed states. Muddy sandstones, siltstones, and mudstones are predominately in the completely decomposed state.

As specified by the URCS, a blow from the rounded end of a 16-ounce ballpeen hammer was used to estimate rock strength. Impact reactions ranged from dent quality (C) to crater quality (D). Moldable quality (E) rocks are most common. According to the URCS, dent quality rocks have an estimated unconfined compressive strength of 3,000 to 8,000 pounds per square inch (psi). Crater quality rocks ranges from 3,000 to 1000 psi, and moldable quality rocks are less than 1,000 psi. Dent quality rocks invariably are conglomeratic sandstone or sandstone; however crater quality and moldable quality varieties of these rocks are common. Siltstones and mudstones are moldable quality in almost all cases.

Discontinuities may indicate directional weaknesses in the rock mass, as well its the ability to transmit water. Here, as observed in outcrop, internal planar separations in the rock mass consist mainly of fractures and bedding planes. At the

Appendix C Weathering and Rock Mass Classification

outcrop scale, essentially all rocks contain intersecting open planes, referred to in the URCS as three-dimensional, open planar separations (E). The in-filling present in some fractures and bedding plane is typically remoldable (<1000 psi) light gray to gray-green clay. Figures 7, 8, and 10 illustrate typical examples of the scale of intersecting discontinuities. The rock mass within the intersecting discontinuities varies from solid random breakage to solid preferred breakage. Solid preferred breakage typically occurs in rock units with closely spaced bedding plane partings commonly found in thinly bedded or laminated sandstones and siltstones.

Actual measurements of unit weights in of different rock units were not conducted. Estimates of unit weights in pounds per cubic foot (pcf) based on the heft of the samples indicate that in most cases the unit weight ranges from 150 pcf (C) to 130 pcf (D) for stained state, dent quality rock specimens. Completely decomposed (moldable quality) rocks are estimated to be less than 130 pcf (E), probably on the order of 120 to 110 pcf. These estimates are consistent with determinations of dry unit weights made for weathered Triassic-age rocks during characterization of the Wake/Chatham site. These measured values are presented in section 2.5, geotechnical characteristics, of the license application (Chem-Nuclear Systems Inc., 1993).






In summary, the relatively more resistant rocks in the borrow pits that form ledges or rock pavements are stained state, dent quality, conglomeratic sandstones and sandstones (URCS CCEC). Partly to completely decomposed units predominate, and include conglomeratic sandstone, sandstone, siltstone, and mudstone (URCS DDED to EEEE). Siltstone and mudstone are almost invariably completely decomposed, and are remoldable with finger pressure (URCS EEEE). In the partly to completely decomposed states these weathering products have engineering properties similar to those of soil. The weathering products of completely decomposed rocks exposed in the floors of the pits were classified in general accordance with ASTM D 2488 - 84 ϵ 1 (American Society for Testing and Materials, 1989). The weathering products of completely decomposed, conglomeratic sandstone and sandstone are typically silty sand and silty sand with gravel (SM), or less commonly, silty gravel (GM). Muddy sandstone can decompose to clayey sand (SC). Siltstone and mudstone typically decompose to silt and clay mixtures, with or without sand (ML, MH, CL and CH).

UNIFIED ROCK CLASSIFICATION SYSTEM
(modified from Williamson, 1984)

DEGREE OF WEATHERING

REPRESENTATIVE		ALTERED	WEATHERED			
			>GRAVEL SIZE		<SAND SIZE	
Micro Fresh State (MFS) A	Visually Fresh State (VFS) B	Stained State (STS) C	Partly Decomposed State (PDS) D		Completely Decomposed State (CDS) E	
UNIT WEIGHT RELATIVE ABSORPTION		COMPARE TO FRESH STATE	NON-PLASTIC	PLASTIC	NON-PLASTIC	PLASTIC

ESTIMATED STRENGTH

REACTION TO IMPACT OF 1 LB. BALLPEEN HAMMER				REMOLDING ¹
"Rebounds" (Elastic) (RQ) A	"Pits" (Tensional) (PQ) B	"Dents" (Compression) (DQ) C	"Craters" (Shears) (CQ) D	Moldable (Friable) (MQ) E
>15000 psi ² >103 MPa	8000-15000 psi ² 55-103 MPa	3000-8000 psi ² 21-55 MPa	1000-3000 psi ² 7-21 MPa	<1000 psi ² <7 MPa
A 	B 	C 	D 	E 

- (1) Strength Estimated by Soil Mechanics Techniques
(2) Approximate Unconfined Compressive Strength

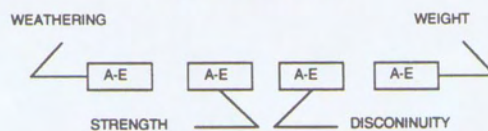
DISCONTINUITIES

VERY LOW PERMEABILITY			MAY TRANSMIT WATER	
Solid (Random Breakage) (SRB) A	Solid (Preferred Breakage) (SPB) B	Solid (Latent Planes Of Separation) (LPS) C	Nonintersecting Open Planes (2-D) D	Intersecting Open Planes (3-D) E
			ATTITUDE	INTERLOCK

UNIT WEIGHT

Greater Than 160 pcf 2.55 g/cc A	150-160 pcf 2.40-2.55 g/cc B	140-150 pcf 2.25-2.40 g/cc C	130-140 pcf 2.10-2.25 g/cc D	Less Than 130 pcf 2.10 g/cc E
--	------------------------------------	------------------------------------	------------------------------------	-------------------------------------

DESIGN NOTATION



Basic elements of the unified rock classification system

Table 3



TRIASSIC MAP UNITS

- ms/si mudstone and siltstone — purple-to-gray-to-tan mottled mudstone and siltstone, locally sandy; lower contact locally gradational with underlying sandy unit; locally contains abundant iron nodules; weathers to a light gray, clayey sediment.
- ss sandstone — white-to-red, medium-to-coarse grained lithic and feldspathic sandstone; locally gravelly at the base; locally bioturbated.
- css conglomeratic sandstone — tan-to-pale red-to-purple conglomeratic sandstone to conglomeratic muddy sandstone; primarily pebble sized clasts of quartz and rock fragments.
- mss/si/ms undifferentiated, interbedded muddy sandstone, siltstone, and mudstone — red-to-brown with interbeds of clast supported sandstone.

MAP SYMBOLS

- geologic contact, solid where exposed or readily inferred from nearby outcrops, dashed where projected or covered, queried where uncertain
- strike and dip of bedding
- strike and dip of fractures
- strike of vertical fractures
- trend and plunge of fold axis
- strike and dip of fault with normal and strike-slip components; ball on downthrown side
- strike and dip of fault with reverse and strike-slip components; teeth on upthrown side
- rake of slickenline on fault plane
- iron nodules
- 8 location number referenced in text (locations 1-7 in south borrow pit)

- SBPF south borrow pit fault
- FA, FB, FC Faults A, B, and C
- N (approx.)
- 0 250 500 ft
- scale is approximate

Plate 1. Bedrock map of the north and south borrow pits (1:3750 approx. scale).



TRIASSIC MAP UNITS

- m/s/si — mudstone and siltstone — purple-to-gray-to-tan mottled mudstone and siltstone, locally sandy; lower contact locally gradational with underlying sandy unit; locally contains abundant iron nodules; weathers to a light gray, clayey sediment.
- ss — sandstone — white-to-red, medium-to-coarse grained lithic and feldspathic sandstone; locally gravelly at the base; locally bioturbated.
- css — conglomeratic sandstone — tan-to-pale red-to-purple conglomeratic sandstone to conglomeratic muddy sandstone; primarily pebble sized clasts of quartz and rock fragments.
- mss/si/ms — undifferentiated, interbedded muddy sandstone, siltstone, and mudstone — red-to-brown with interbeds of clay supported sandstone.

MAP SYMBOLS

- geologic contact, solid where exposed or readily inferred from nearby outcrops, dashed where projected or covered, queried where uncertain
- strike and dip of bedding
- strike and dip of fractures
- strike of vertical fractures
- strike and dip of fault with normal and strike-slip components; ball on downthrown side
- trend and plunge of fold axis
- rake of slickenline on fault plane
- iron nodules
- location number referenced in text (location 8 located in north borrow pit)

SBPF south borrow pit fault
FA, FB Faults A, and B

Geologic mapping by Richard M. Wooten, Timothy L. Davis, Timothy W. Clark, and Kathleen M. Farrell, 1992-1996.

0 125 250 ft
 scale is approximate

1 **2** **3** **4** **5** **6** **7**

SBPF **MS/ST** **MSS/ST/MS**

SHEKON HARRIS RESERVOIR

N (approx.)

Plate 2. Bedrock map of the south borrow pit (1:2145 approx. scale). North Carolina Geological Survey Open-File Report 96-3